Liquid Crystal Based Sensors for the Detection of Heavy Metals

By

Zehra Javed Malik

School of Chemical and Materials Engineering

(SCME)

National University of Sciences and Technology

(NUST)

2016

Liquid Crystal Based Sensors for the Detection of Heavy Metals

Zehra Javed Malik
NUST201362352MSCME62319F

This thesis is submitted as a partial fulfillment of the requirements for the degree of

Masters of Science (MS) in Nanoscience and Engineering

Supervisor: Prof. Dr. Zakir Hussain

School of Chemical and Materials Engineering (SCME)
National University of Sciences and Technology
H-12 Islamabad, Pakistan

June, 2016

Thesis SubmissionCertificate

This is to certify that work in this thesis has been carried out by **Ms. Zehra Javed Malik** and completed under my supervision in Nanosynthesis Laboratory at School of Chemical and Materials Engineering, National University of Sciences and Technology, H-12, Islamabad, Pakistan.

Supervisor _____

Prof. Dr. Zakir Hussain
Materials Engineering Department
National University of Sciences & Technology, Islamabad.

Submitted through

_____

Prof. Dr. Mohammad Mujahid
Principal/Dean,
School of Chemical & Materials Engineering
National University of Sciences and Technology, Islamabad.

Dedicated to

Ammi, Abu, family, friends and everyone who supported this.

Thank you for sticking by

Acknowledgements

All praises to Almighty Allah, the authority of knowledge and creator of resources, skills and opportunities.

I would like to extend my heartfelt gratitude to my supervisor, Prof. Dr. Zakir Hussain, (SCME), for his patience, support and guidance throughout the study. I am also thankful to my thesis GEC members; Dr. Iftikhar Hussain Gul (SCME) and Dr. Shahrukh Abbas (ASAB), for their valuable suggestions.

I would also like to acknowledge the various roles played by many, many people to give this project a tangible outcome and feel deeply ingratiated to everyone for their support.

Technical Assistance
Ms. Farah Qazi (SCME)
Ms. Saman Zaidi (SCME)
Mr. Shams-ud-Din, SEM Lab (SCME)
Mr. Khurram, XRD Lab (SCME)
Mr. Zafar Iqbal, Surf Eng. Lab (SCME)
Mr. Khalid Akbar, Microscopy Lab (SCME)
Mr. Zeeshan, Chemistry Lab (SCME)
Mr. Abdul Qadeer, Corrosion Lab (SCME)

Administration, SCME
Prof. Dr. M. Mujahid, Principal, SCME
Prof. Dr. M. Shahid, HoD (ME), SCME

Faculty, NUST
Prof. Dr. Zakir Hussain (SCME)
Dr. Amir Habib (SCME)
Prof. Dr. Nasir M. Ahmad (SCME)
Dr. Israr Qadir (SCME)
Dr. Iram Mahmood (SCME)
Dr. Shahzad Hussain (SCME)
Dr. Nosheen Fatima (SMME

In the end, I feel blessed to have a very strong and reliable support system of friends and colleagues who have been an extensive, readily available source of technical expertise, dynamic ideas, and sound advice during the lab work and thesis write-up. I am grateful to *Sundas Khalid, Khazima Muazim, Syeda Qudsia, Misbah Nazir, Haleema Tariq Bhatti, and Ayesha Tabriz* for their consistent help, caring attitude and cheerful company during my stay at the university. *Aqdas* and *Miriam* thank you for your constant support.

Most importantly, none of this would have been possible without the love and patience of my family. All of them have been a constant source of inspiration, concern, support and strength all these years.

Zehra Javed Malik

Abstract

Arsenic related toxicity contributes heavily to the disease burden globally, resulting in a dire need to discover new and more sensitive means of both; detecting and measuring it. Subsequently, integrating the concepts of nanotechnology and liquid crystalline materials, a new breed of sensors is being suggested. Herein, based on the already reported adsorption affinity cobalt ferrite nanoparticles display for arsenate, the perturbation sensitive and optically anisotropic liquid crystals (LCs) were suggested as a means of detection, transducing and amplifying the said interaction. To test this hypothesis, cobalt ferrite nanoparticles were foremost synthesized and characterized using XRD and SEM. This was followed by establishing optimal concentrations of surfactant and nanoparticles in order to achieve stabilized LC sensing platform. Finally, upon testing varying concentrations of sodium arsenate (1000ppm, 500ppm, 100ppm, 1ppm), optically distinguishable results were observed when viewed under polarized optical microscope, suggesting this sensing platform to exhibit the feature of sensitivity for varying range of arsenate.

Key Words: *Liquid crystals, sensing, arsenic, heavy metal, detection, cobalt ferrite, nanoparticles*

Table of Contents

Table of Contents

List of Figures

List of Figures

List of Figures

List of Tables

List of Abbreviations

As	Arsenic
AFS	Atomic Fluorescence Spectroscopy
AAS	Atomic Absorption Spectroscopy
R-FS	X-Ray Fluorescence Spectroscopy
ICP-MS	Inductively Coupled Plasma-Mass Spectrometry
LC	Liquid crystal
5CB	p-n pentyl-p-cyanobiphenyl
AFM	Atomic force Microscopy
QCM	Quartz crystal microbalance
CAM	Coupling Agents Molecules
DMOAP	N, N-Dimethyl-N-octadecyl-3- aminopropyltrimethoxysilyl chloride
CTAB	Cetyltrimethylammonium bromide
Span 80	Sodium monoleate 80
PBS	Phosphate buffer saline
TDS	Total dissolved solutes

Chapter 1. Introduction

Arsenic (As) related toxicity has presented itself as a problem of catastrophic proportions affecting an estimated 150 million people worldwide, of which 110 million live within the 10 countries of South and South East Asia, Pakistan being one of them [1].Currently, the biggest source of arsenic toxicity, both due to natural and anthropogenic activities, is the contaminated groundwater. Prolonged exposure and usage of such water poses threat to sustainable agriculture along with human health, adding severely to the disease burden.

Resultantly, with arsenic being non-biodegradable and staying indefinitely within the environment, there is a need for its effective monitoring, measurement and remediation in soil and groundwater. Arsenic toxicity is largely governed by its speciation and it's most important toxicity causative forms in drinking water are the inorganic variants. These include both; arsenite (As^{III}) (H_2AsO_3, $H_2AsO_3^-$) and arsenate (As^{IV}) H_2AsO_4 −, $HAsO4^{2-}$. Resultantly, arsenate, arsenate anions, along with the neutral arsenite have been the focal targets for field analytical assays [2].

Laboratory assays for arsenic measurement exist and require certain pre-processing wherein all of the arsenic in collected sample is transferred to an acidic solution. Subsequently, this sample is then analyzed by one of the many accepted assays [3]. Although these analytical assessment methods have resulted in sensitive detection of heavy metal ions yet they exhibit several inadequacies such as the need for complex, expensive and elaborate equipment along with laborious and sophisticated sample preparation steps. This markedly limits their utility as on-site arsenic detection platforms that otherwise require portable, cheap, convenient, sensitive and rapid means of detection.

In this context, liquid crystals (LC) that are lately being studied as intelligent sensing materials, have emerged as a potential candidates that can be explored in order to replace conventional analytical means for on-site detection. LCs are largely organic materials showing both; an intermediate state of matter along with properties, existing between solid (crystalline) and liquid (isotropic) phases. They are known for exhibiting anisotropic physical properties like that of a solid while displaying flow-like properties of liquid matter. From an application point of view, the already well exploited useful

properties of the liquid crystalline phase are: anisotropy, selective absorption of plane polarized light along with the property of being influenced by electric and magnetic fields. Furthermore, these materials show sensitivity towards any minor changes in surface energy or in the surrounding environment [4]. This change could be consequence of presence of foreign species, occurrence of binding events or any other physical, chemical perturbation. Furthermore, LCs show potential to amplify and transform otherwise negligible molecular occurrences within their vicinity into macroscopic measurable signals [5]. This responsive nature combined with the optical anisotropic behavior, wherein when observed under cross polarizers, LCs may appear dark or bright based on their orientation [6], forms the basis of using LCs for optical sensing.

As a result of such stimuli sensitive and optically anisotropic nature of LCs, they have been extensively employed for myriad of sensing applications including both; chemical as well as biological sensing [7, 8, 9, and 10]. Detection of heavy metals such as Hg^{2+} and Cu^{2+} by means of various detecting molecules such as biomolecules (like oligonucleotides) along with other complementary chemical moieties, within LC system has already been reported [11, 12]. And although these investigations report good sensitivity, they also indicate of a need to find cheaper, easier to produce/process alternatives offering improved sensitivity, selectivity along with accuracy to already suggested detecting molecules. This research effort aims to tackle detection of heavy metal, i.e. sodium arsenate, within LC based sensing system by offering such an alternative.

Subsequently, in our study, principles of LC are fused with that of nanotechnology. The aim was to harness the size/surface area resultant enhanced properties of nanoparticles along with the multiple advantages and potential they are reported to extend to the LC system [13]. As a result, in this investigation the already well reported adsorption affinity of arsenate for cobalt ferrite nanoparticles has been manipulated [14, 15].

So stringing it all up, we hypothesize that based on the disturbance caused by already reported arsenate adsorption onto cobalt ferrite nanoparticles, perturbation sensitive and optically anisotropic LC, are to change orientation which in turn effects the amount of light leakage when viewed under polarized microscope. This specific interaction, similar to previously reported LC based sensing studies for other interactions [16, 17, 18, 19, 20], was forecasted to cause perpendicularly aligned LC

(dark image/complete light blockage) to transition ultimately to a parallel alignment (bright image/complete light leakage), with series of intermediate angles of tilt shown by LC in between, displaying varying degree of luminosity and resultantly forming the basis of our LC based optical sensing.

In order to test this hypothesis we laid down a series of sequential objectives which are given below:

- Synthesis & Characterization of cobalt ferrite nanoparticles
- Successful embedding of nanoparticles in the LC based sensing platforms
- Detection of sodium arsenate within nanoparticle stabilized LC sensing platforms

Chapter 2. Review of Literature

2.1 Heavy Metal Toxicity

Metals ions having atomic weights in the range of 63.5 to 200.6 along with specific gravity of less than 5.0 g/cm^3 [21] are categorized as heavy metal ions. Heavy metals are non-biodegradable and as a result exist in the ecological systems indefinitely, exposing all species to increased amounts of contamination. These metals exhibit an ability to form complexes, with ligands of various biological matter comprising oxygen, sulphur and nitrogen. Resultantly, changes in the molecular arrangement of proteins, denaturation of enzymes or breaking of hydrogen bonds can occur. Such molecular changes can in turn lead to myriad of toxicological and carcinogenic effects [22].

Subsequently, safe limits have been defined for drinking water by different organizations world over, chiefly; World Health Organization (WHO) and Environmental Protection Agency (EPA), based on the toxicity data and scientific studies [23].

2.1.1Arsenic Toxicity

Arsenic- Forms and Occurrence

Arsenic (As) is naturally present in the environment and appears highly toxic to all life forms. It is a crystalline metalloid with features laying between that of metals and non-metals. It is the 20^{th} most occurring trace element in the earth's crust while ranks 12^{th} most common element in the human body [24]. Arsenic exists largely in four oxidation states – arsenate (As^{V}), arsenite (As^{III}), arsenic (As^{0}), and arsine (As^{-III}) and its solubility is dependent on the ionic environment along with pH. Among the various arsenic species, the As^{V} is reported to be thermodynamically stable state in aerobic water, while As^{III} is predominant in redox environments. Furthermore, arsenic can be present in the environment in various chemical forms [25]. The principal source of as in the environment is its release from As-enriched minerals. The sources of As contamination includes natural (dissolution of As compounds into the water by geochemical factor) as well as anthropogenic activities (mining and smelting, industrial processes etc.). Subsequently, existence of As in fresh waters, marine waters, ground

and drinking water along with soil and food stuffs is frequently reported. Exposure to contaminated drinking water is the key source of As toxicity within human population while those not exposed directly to raised levels of As in drinking water can still be a victim of this toxicity i.e. by usage of food grown in As-contaminated soil. So all such exposures result in health-threatening problems for millions [26].

Health Hazards

The numerous debilitating effects of As poisoning on human health include melanosis, keratosis, edema, gangrene along with skin cancer. Keratosis and melanosis are the most common skin related pathological presentations to be reported.

Furthermore, prolonged exposure to inorganic As causes plethora of disorders, adversely affecting body throughout i.e. digestive, respiratory, cardiovascular, hematopoietic, endocrine, renal, neurological as well as reproductive system/s [27].

2.1.2 Current Technologies and Research Trends for Arsenic Detection

Existing standard techniques for detection of trace amounts of heavy-metals require sophisticated techniques such as but not limited to atomic absorption spectroscopy (AAS), inductively coupled plasma-mass spectrometry (ICPMS), mass spectroscopy (MS), X-ray fluorescence spectroscopy (R-FS) and potentiometric methods [22]. Advances in a variety of analytical instruments have shown varying success. However, the fundamental goal of developing on-site assays that consistently and accurately detect and measure arsenic has yet not been achieved .Field assays, though are relatively inexpensive and can produce a large number of screening results in a short period of time as of yet lack the desired sensitivities to accurately measure low amounts of heavy metal ions [3].

Resultantly, new avenues are being explored to achieve enhanced sensitivities with researchers identifying and stringing concepts from various fields. An area generating a lot of interest is the field of nanotechnology. Nanoparticles, with particle sizes of less than 100nm, present with plethora of interesting and uniquely attractive features making them very lucrative for various technologically advanced applications [28].

For sensing, nanoparticles have been gathering a lot of attention, primarily due to the improved properties they display as a consequence of small size and enhanced surface area. The introduction of nanostructured materials, including but not limited to quantum dots (QDs), magnetic nanoparticles along with noble metal nanoparticles, which improve sensibility, selectivity as well as reproducibility, has contributed greatly to improve the existing detection limits achieved while allowing the possibility for miniaturization of devices.

Nanostructured materials have been widely reported both for recognition as well as remediation of heavy metals. Adsorption of both; As(III) and As(V) by nanocrystalline TiO_2 particles has been reported on numerous occasions [29, 30]. Furthermore, iron based nanoparticles such as zero valent iron, maghematite [31] and various ferrites [32] have also been investigated for the adsorption affinity displayed by them for various arsenic forms.

2.2 Liquid Crystal Based Sensing

2.2.1 Liquid Crystals

Matter exists broadly in four chief states i.e.; solid, liquid, gaseous, and plasma. Each of these states differ in terms of distribution of atoms and degrees of freedom exhibited by molecules. However, an interesting class of materials exists that possesses properties that overlaps this otherwise discrete grouping. Liquid Crystals (LC) are one such category of materials

As the name suggests, LC refers to crystals that are liquid in nature, displaying properties between that of solid and isotropic liquid phases. These are primarily organic materials comprising of molecules exhibiting solid-like anisotropic and liquid-like flowing properties. This exquisite feature gives them unique set of properties and has made them appropriate for numerous applications [33].

2.2.2Type of Liquid Crystals

The liquid crystal (LC) phases are fundamentally categorized depending on the temperature or on the concentration of the molecules within a solution, as well as on

the shape of the constituting molecules. LCs can be largely subdivided into two broad categories i.e. thermotropic and lyotropic LCs.

Thermotropic Liquid Crystal

Thermotropic liquid crystal phases are formed between the crystalline and the isotropic phase by changing the temperature. This phase of LC is dependent on the chemical composition of the various discrete components within the mixture. Thermotropic LCs display different phases when heated above a specific temperature at which the crystalline arrangement of the crystal is disturbed. Heating it above its liquid crystalline range results in further disruption of molecular organization, before eventually transitioning to normal isotropic liquid. Thermotropic liquid crystalline materials exhibit characteristics associated to their molecular structure, which consist of two parts, namely the core and side chain. The core is a rigid body which is attributed with shape anisotropy of the molecule, while the side chain is a flexible segment, giving the molecule feature of mobility. Most of the existing commercial electro-optic devices such as displays (LCDs) and digital watches are reported to use thermotropic LCs [34, 35].

As stated previously, thermotropic LCs displays different phases upon temperature change. These sub-phases are arranged according to the degree of order they exhibit between solid (most ordered) and the isotropic liquid phase. Thermotropic LC sub phases include, Nematic Phase, Smectic Phase and Cholesteric Phase.

Nematic Liquid Crystals

Nematic liquid crystals are LCs that display orientational ordering but lack long-range positional ordering. The nematic phase is the least ordered liquid crystalline phase among various LC thermotropic phases. Herein the molecules have freedom to flow though these molecules yet maintain long-range directional order. Nematic LCs mostly have a single, slightly longer preferred axis, known as the principal axis, along with two perpendicular axes which are equivalent and mutually perpendicular. The nematic liquid crystals are the most widely used liquid crystalline materials and are known particularly for their usage for device applications including LCDs [36].

Smectic Liquid Crystal

Smectic liquid crystalline phase is the phase closest to the solid (crystalline) state of matter. It comprises of stratified layers with two-dimensional (2 D) ordering between the layers. The molecules within each layer display both; orientational as well as positional order between them. However, the inter-layer forces within smectic liquid crystals are relatively weak in nature. This is why the liquid crystal is fluid in smectic phase. Furthermore, there are various phases in this family such as SA, SB, SC, SG, SH, SJ, and SK where S represents the smectic phase and the suffix denotes the type [37].

Cholesteric /Chiral Nematic Liquid Crystals

Cholesteric /Chiral Nematic Liquid Crystals are nematic LCs the addition of constituting optically active molecules as well [1]. This is achieved by adding a slight amount of chiral dyes to a normal nematic Because of presence of optically active molecules, the director experiences a twist about the axis normal to the preferred molecular directions.

Lyotropic Liquid Crystal

The second major type of LC includes Lyotropic liquid crystal phases, which can be obtained by changing the concentration of the organic solutes in the solution. Lyotropic liquid-crystalline materials do not necessarily exhibit shape anisotropy, but rather show the feature of self-assembly which in turn depends on the solute concentration in a solvent. Lyotropics characteristically form micelle arrangements, and usually find application in cosmetic, beauty and in detergent industries [37]

Anisotropic Physical Properties

An important consequence of the anisotropic shape of liquid crystal molecules is their anisotropic physical properties. Resultantly in nematics each of the measured physical property tends to have two different values depending on the direction of measurement i.e. parallel or perpendicular to the principal axis given by the director.

Dielectric Anisotropy

The anisotropic nature of the liquid crystalline material affects their response to an applied electric field. The nematic LCs possess two different values of dielectric constants i.e. one for a field oscillating parallel to the optical axis while the other for a field perpendicular to it. Furthermore, the sign of the dielectric anisotropy will define whether the nematic molecule will lie along the direction of the applied electric field or perpendicular to it [36].

Optical Anisotropy

The optical properties of anisotropic liquid crystalline materials also vary with direction. In the case of nematic LCs two refractive indices are observed. One of the refractive index is measured in parallel while other is measured in perpendicular direction. The birefringence (i.e. optical anisotropy) of LCs represents the difference between the two refractive indices [36].

2.3 Liquid Crystals as sensing materials

2.3.1 Sensing Properties

Liquid crystalline molecules have been termed as smart materials as a result of their stimuli sensitive nature. These optically anisotropic molecules are reported to show response to slightest of disturbances in their vicinity brought about by any physical or chemical change. Furthermore, amplifying and transducing a signal are also capabilities demonstrated by LCs [34].

2.3.2 Types of Liquid Crystal Sensors

Applicability of liquid crystal as sensing material may be broad since they can be coated onto various transduction platforms. Example include optical platforms such as; optical waveguides surface plasmon resonance, interferometers; electrical platforms including capacitive transducers; mechanical platforms like atomic force microscopy (AFM) cantilevers and quartz crystal microbalances (QCM) [38].

2.4 Optical Liquid Crystal Sensing

2.4.1 Sensing Principle

The basic principle behind LC based sensing is simply based on both the ability of LC to be sensitive to any slightest of changes in its surrounding chemical environment as well its ability to influence absorption of plane polarized light resulting in varying degree of light leakage. Resultantly, slightest disruption of aligned LC brought about by the specific interaction of analyte and detecting molecule/receptor causes the LC to change orientation which in turn effects the amount of light leakage which causes optically different visuals being captured under polarized optical microscope. Figure 1 below presents a simple schematic explaining the sensing principle sequentially.

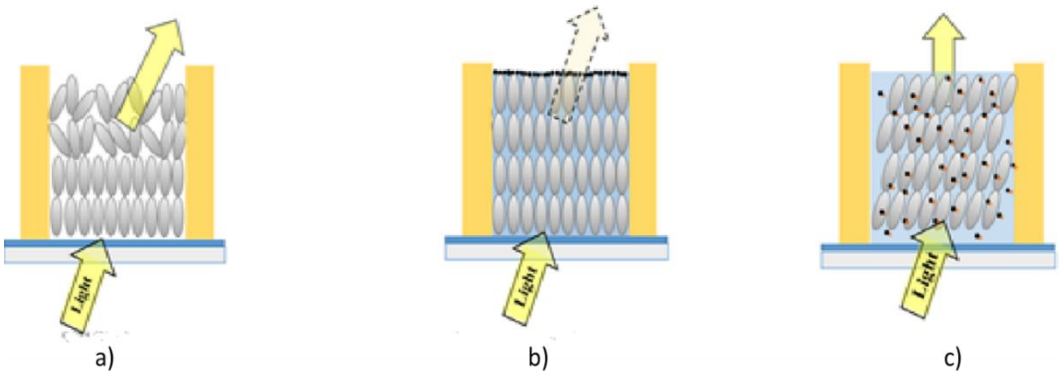

Figure 1: Schematic diagram explaining the LC based sensing principle: a) originally partially aligned LC, b) Addition of detection molecules and surfactant resulting in perpendicular alignment, c) addition of analyte results in disruption of LC

2.4.2 LC Surface Alignment- Methods and Factors Involved

Liquid crystals (LCs) have gravitated interest of researchers due to their anisotropic physical properties and easy control of their orientation by external fields including electric, magnetic and light. Subsequently, in order to make use of this anisotropic behavior of nematic LCs they need to be foremost aligned uniformly along a preferred direction. Such uniform alignment of the LCs can be achieved by means of

applying of an external field; electric, magnetic or light, as well as by the interaction of the LC with a solid surface and interaction with other molecule/s. [36]

Liquid crystal alignment is essential in almost all liquid crystal based devices. Generally, LCs can be aligned at solid substrate surfaces. The interaction between molecules of LC is dictated by long-range interactions. Resultantly, the alignment of these molecules at the surface's monolayers can be easily conveyed to the bulk resulting in uniform alignment. Additional forces that impart alignment comprise of dipole interactions with the surface, elastic forces because to surface morphology along with chemical interactions with the chemical groups on surface. Of these, chemical interactions are known to play the dominant role in surface alignment [37].

Furthermore, the balance between the surface tension of LC ($_{y}$L) and the surface tension of solid ($_{y}$S), when LC is dropped on a solid surface, will determine the direction LC molecules will prefer to align with. These elongated molecules tend to order themselves perpendicular to the surface, when $_{y}$ L > $_{y}$S, in order to minimize surface energy (in this case intermolecular forces between LCs dominate).While when $_{y}$ L < $_{y}$ S, the LC molecules chose to align themselves parallel to the surface of substrate [5]. A third case exits wherein when L ~ S the LC molecules adopt tilted alignment.

Moreover, LC alignment is classified according to the orientation they display i.e. either homeotropic (vertical), planar (parallel) or tilted alignment. In homeotropic alignment LC molecules are aligned perpendicular to the surface, in planar alignment these molecules are parallel to the surface while in the tilted alignment, LC molecules lie between 0 and 90°.

2.4.3 Components Involved in LC Based Sensing

Liquid crystal (LC) based optical sensor comprises of certain basic components which include the substrate used, bottom aligning layer, liquid crystalline material, aqueous-air interface aligning surfactant along with polarized optical microscope. In the sections to follow, each component is discussed.

Liquid Crystalline Material

Liquid crystals (LCs) as already stated are broadly of two types i.e. thermotropic and lyotropic. Recent literature survey shows that most research efforts have employed thermotropic liquid crystal p-n pentyl-p-cyanobiphenyl (5CB) as signal amplifier. 5CB presents with handful of advantages such as convenient room temperature nematic range along with high chemical stability even in the presence of molecules of water vapor and oxygen, making it a preferred choice. Moreover, this nematic LC has a large positive refractive index anisotropy which makes it appropriate for amplification because of a phase transition into the isotropic phase [38].

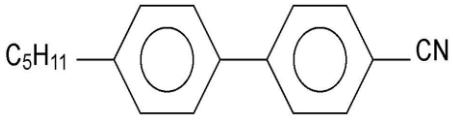

Figure 2: Structure of p-n pentyl-p-cyanobiphenyl (5CB)

Substrate

Substrates are a chief component of LCs based sensing platform, especially from a technological and device fabrication point of view. As of yet, most of the research efforts have been carried out by using of microscopic glass (borosilicate) slides as bottom substrate. However, reports have stated the use of polymer based bottom substrates. Basically a substrate can be made from any suitable material that shows compatibility with the alignment layer along with the physical property that is being measured. For cases where physical property to be measured is optical or is measured by optical means, the substrate may be a transparent material such as glass [38].

Because of observations that the cleanliness of the substrate is essential for the study of surface alignment, there is a need to employ cleaning protocol which repeatedly results in reproducible and uniform chemical surface, especially one which results in a surface clear of organic contamination. Subsequently, the effectivity of cleaning procedures ought to be constantly monitored by an appropriate technique and by carrying relevant controls throughout experimentation. Previously conducted studies reported that solvents, detergents and non-oxidative heat treatments are substantially ineffective in clearing high energy surfaces from organic contaminants.

Instead it has been suggested that strongly oxidizing conditions are essential to fully clear organic residue [39]

Surface coupling agent

Another significant component within LC sensing platforms is the substrate alignment/surface coupling agent. Basically in order to fully align the LC with bottom substrate an alignment agent is needed. It is desirable to find materials that not only have an orienting action on LC molecules but also bond permanently to the substrates. Surface coupling agents have these properties. Coupling agent molecules (CAM's) for aligning LCs with substrate should ideally possess at least two different kinds of functional groups. One of these group should display chemical reactivity with the substrate while the other ought to be the aligning group which results in such an interaction with LC molecules that brings about the preferred orientation [40].

Furthermore, surface coupling agents most widely used include organosilanes, because of their ability to provide stable bonding between dissimilar surfaces. Alkoxysilane monomers have a general formula $RSiX_3$ and are a well-known class of CAMs. In this general formula, *R* is an organofunctional group attached to the silicon atom in a stable manner, having an orienting effect on LCs while X denotes hydrolyzable groups centered upon silicon. Furthermore, the strength of the substrate-silane bonding depends on the chemical nature of the substrate, that of silane as well as the deposition conditions used to deposit silane.

Surfaces coated with organosilane are reported to be remarkably stable in the presence of moisture [22], making it desirable for LC based devices. Moreover, the chemical bonding between the surfaces and organosilane also prevents adsorption of other molecules**.**

N, N-Dimethyl-N-octadecyl-3- aminopropyltrimethoxysilyl chloride (DMOAP) is a very widely used surface coupling agent. It is known to be stable in the presence of moisture and they provide the constant value of critical surface tension desired for liquid crystal device structures, LC colloidal applications and meta material application [40].

Surfactant

Surface active agents, commonly known as surfactants, are chemicals that display a tendency to physically adsorb at an interface or surface, resultantly altering the energy dynamics at that surface. A LC in contact with a substrate having surfactant coating is expected to align differently than if it was to, to a substrate without coating Subsequently, with such an essential role in LC alignment, research attempt to better understand the effect and dynamics of surfactants on LC alignment were initiated by the findings of Haas *et al.* wherein thin layers of the liquid-crystalline MBBA was reported to display homeotropic orientation when doped with trace amounts of polyamide resin (Versamid 100). This study concluded that the surfactant properties of the resin molecules aided in the homeotropic alignment of LC.

However, it is important to note that a given surfactant will not necessarily display the same aligning action for all liquid crystalline materials or for all given substrates. The orienting action is reported to depend on the specific chemical structure of the substrate, surfactant as well as that of LC [39].

The most widely used surfactants for aqueous-air interface alignment of LCs have been the lipids. However other surfactants such as TritonX-100 and Tween80 have also been reported.

2.5 Optical Liquid Crystal Sensing Applications

Liquid crystals have been reported for sensing of wide variety of molecules. These anisotropic materials have gained quite popularity in the field of biosensing due to their properties of amplifying molecular events to macroscopically detectable signals. Various biological molecules such as enzymes, glucose, lipids along with proteins etc. have been sensed using liquid crystalline materials. Viruses and bacterial detection has also been investigated in this context [5, 41, 42, 43]

Furthermore, chemical agents such as xylene, naphthalene, glutaraldehyde, butylamine etc. are reported to be sensed with LC as medium of detection. These studies have met with varying success in terms of sensitivity and selectivity, showing encouraging results for future exploration [44, 45 46, 47]

Finally, heavy metal detection has also been an area that has been researched using stimuli responsive LCs. Largely heavy metals explored so far include Hg^{2+}, Co^{2+} along with Cu^{2+}. LC based sensor for the detection of Cu+2 ions has been reported by Hu *et al.,* wherein surface immobilized urease was responsible for detection. Herein upon treatment with UV, 5CB immersed in a solution of urea showed an optical response from bright to dark transition upon interacting with surface immobilized urease. In the presence of Cu^{+2} ions, urease activity was blocked and so a transition from homeotropic-to planar i.e. dark to the bright was observed [48].

In another study, detection of mercury ions was reported by employing oligonucleotides showing specific binding with Hg^{+2} (Yang *et al.,* 2012). The presence of Hg^{+2} ions induced conformational changes on the originally hairpin structure of oligonucleotide to a duplex like complex, which caused a disruption that caused homeotropically aligned LCs to transition to planar arrangements, resulting in dark to bright changes optically [11].

Detection of Cu^{+2} and Co^{+2} ions was achieved by Han *et al.,* wherein an optical acid doped LCs incubated with heavy metals showed dark to bright appearance indicating the presence of stated metal ions. The interaction of metal ions with specific chemical moieties on the stearic acid resulted in disruption of LCs, ultimately causing a change in orientation which in turn was visible by the dark to bright transition noted optically [12].

Chapter 3. Materials and Methods

3.1 Cobalt Ferrite Synthesis

3.1.1 Materials

$Co(NO_3)_2 \cdot 6H_2O$ (75 ml of 0.1M), $Fe(NO_3)_3 \cdot 9H_2O$ (75 ml of 0.2M), NaOH (75 ml of 3M), Cetyltrimethylammonium bromide, CTAB (95-98%) were all purchased from Sigma-Aldrich. All reagents were of analytical grade. Deionized water was used for all solution making and later washing of nanoparticles as well.

3.1.2 Synthesis

Synthesis of cobalt ferrite nanoparticles was achieved by adapting the protocol reported by Gul *et al.,* [49]. Foremost, solutions of $Co(NO_3)_2 \cdot 6H_2O$ (Sol A) and $Fe(NO_3)_3 \cdot 9H_2O$ (Sol B) in their desired stoichiometry were prepared separately in deionized water while providing magnetic stirring for almost 5 minutes. Next, Sol A was poured into Sol B, and stirred magnetically for 10minutes. This aqueous solution was then heated up till 35ºC after which CTAB (0.281g) was added as a surfactant to provide stearic hindrance during particle synthesis in order to achieve well dispersed nanoparticles. Once this was added and mixed, this aqueous solution was allowed to heat up to 85ºC under constant stirring. Upon achieving this temperature, precipitating reagent, NaOH (with a temperature of 85ºC), was mixed into metal solutions. This mixture was then provided with constant stirring and the temperature was maintained for the next 45 minutes. After the desired time, heating was switched off and magnetic stirring was continued till room temperature was attained. The precipitates were thoroughly washed with deionized water several times until a pH of 7 was achieved. The product was dried overnight in an electric oven at 110ºC to remove water contents. Finally, the sample was ground using mortar and pestle after which it was placed for sintering in a muffle furnace at 500ºC for 7 hours [49].

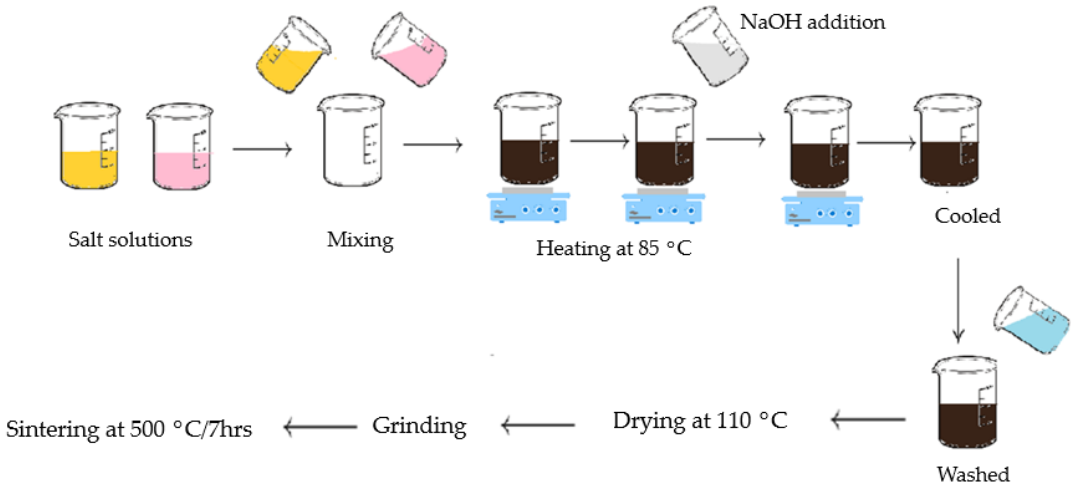

Figure 3: Schematic representation of synthesis of Cobalt Ferrite nanoparticles via Co-precipitation method

3.1.3 Characterization

X-Ray Diffraction

X-ray diffraction (XRD) pattern for the sample was performed and recorded. For this finely ground and dried powder was used as sample. The X-ray diffraction (XRD) pattern was obtained on a STOE Powder X-ray diffractometer θ-θ (operating voltage 40 kV and current 40mA) utilizing a scanning rate of 0.5° min^{-1} ranging from 5° to 80° (2θ) with Cu Kα radiation (λ = 1.5418 Å).

Scanning Electron Microscopy

Scanning electron microscopy was performed in order to assess particle morphology and size. Sample for this assessment was prepared by making dilute and well dispersed solution of the ferrite using ultrapure water as solvent followed by to allow uniform dispersion. After sonication, a drop of sample was placed on the metal grid and was allowed to dry in ambient light. The sample was then placed in JFC-1500, Ion sputtering device, 250 Å, to allow gold coating. Samples were analyzed using JSM-6940A, Analytical SEM, and JEOL-Japan.

3.2 Optical Testing

3.2.1 Materials

Glass microscope slides were purchased from VWR (Germany). N, N-Dimethyl-N-octadecyl-3- aminopropyltrimethoxysilyl chloride (DMOAP), 4-cyano-4'-pentylbiphenyl (5CB, concentrated Sulphuric acid (95-98%), hydrogen peroxide (30% w/w in water), Sodium monoleate 80 (Span 80), phosphate buffer saline tablets, acetone (98-99%) sodium arsenate ($Na_2HAsO_4.7H_2O$) 98% were all purchased from Sigma Aldrich (Germany). Gold grids (150 mesh size) were purchased from Plano GmbH (Wetzlar, Germany). All the chemicals were used as received .All aqueous solutions were prepared and washing steps were done using ultrapure water (Conductivity: 0.0055µSiemens, Total dissolved solutes; TDS: 0.00) throughout the study. The solutions used are mentioned in Table 1.

Table 1: List of solutions prepared

Solution Prepared	Protocol
Piranha	Added 10ml of 30% H_2O_2 slowly in 30ml of conc. H_2SO_4 (Ratio 3:1 H_2O_2:H_2SO_4). Note: This is a highly flammable solution which is to be stored in a tightly secured reagent bottle and should be handled carefully when being used.
DMOAP	357.1µl of DMOAP was added in 150ml of ultrapure water. This solution was poured from one beaker to another multiple times in order to create froth. This solution should be used within 3-4 days of making.
PBS	Single tablet of PBS was added in 100ml of ultrapure water. The solution was sonicated in order to completely dissolve.
Span 80 (1mM)	21.4µl of Span 80 was added to 50ml of ultrapure water. This mixture was sonicated well until a uniform milky dispersion was achieved.
$CoFe_2O_4$ (1mM)	2.35mg of CoFe2O4 nanoparticles were added in 10ml of ultrapure water and was sonicated well until a uniformly dispersed solution was achieved.
Sodium Arsenate (1000ppm)	Solution was prepared by dissolving 42mg of sodium arsenate in 10ml of ultrapure water.

Optical microscope specifics

A polarized optical microscope (Leica) was used to obtain textures of 5CB in liquid crystal based sensor. All the images were recorded by using 10X digital camera attached to polarized optical microscope 100 % transmittance was set without sample and 0 % transmittance when the source of light was switched off [50].

3.2.3 Preparation of Optical LC Based Sensor

Glass Slide Activation

Glass slides were foremost immersed in Piranha solution for 20 minutes, providing them with the strong oxidizing conditions for cleaning. Next after washing with ultra-pure water and drying them using an industrial dryer, the slides were given an acetone wash. And finally after another round of washing and drying, the slides were kept in DMOAP solution for 5 minutes. After this the slides were dried. These DMOAP functionalized slides were ideally used for testing within 2 days of functionalization.

Note: In each step above, washing was done using ultra-pure water and drying of slides was done using an industrial dryer, the latter being set at its maximum heat level. Slides were covered with petri dishes to avoid contamination during storage.

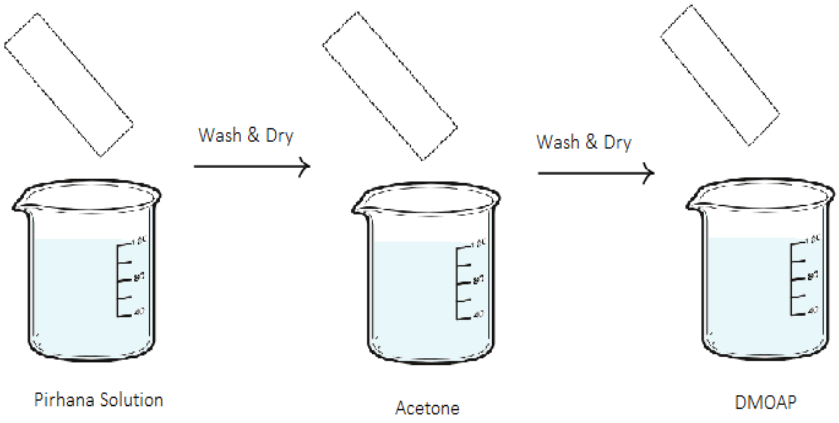

Figure 4: DMOAP activation of microscopic glass slides

Annealing of Liquid Crystal on Gold Grid Laden Activated Glass Slides

Foremost, TEM gold grids (150 mesh), which provide support to the nematic liquid crystals on DMOAP coated slides, were washed prior to use. They were rinsed with acetone and ethanol, 3 times each. These were then given a final wash with ultra-pure water followed with ethanol and lastly were dried in an electric oven at 80ºC.

Washed and dried TEM gold grids were placed on DMOAP activated glass slides using clean micropipette tips to position them carefully on the slide. A maximum of 4 grids were placed on each functionalized slide.

Next, almost 2µl of 5CB was carefully dropped on each grid on the DMOAP coated slide using micropipette. Excess of 5CB was removed using capillary action of micropipette tip.

Finally these 5CB laden slides were placed on a hot plate and subjected to heating for less than a minute at 40ºC. Subsequently these were allowed to cool down to room temperature while being carefully covered with petri dishes to avoid any contamination or disturbance. In order to achieve uniform homeotropically aligned 5CB, the temperature was kept above the phase transition temperature i.e. 35 °C [50].

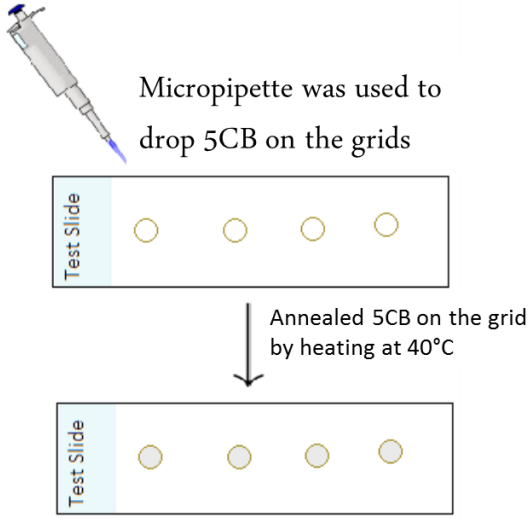

Figure 5: Annealing of 5CB on Gold Grid Laden Activated Glass Slides

Checking of Prepared Optical Sensing Platform

Above fabricated sensor (glass slide based sensing platform) were observed under a polarized optical microscope to assess their viability for further usage. Any gold grid with improper alignment of LC was rejected manually.

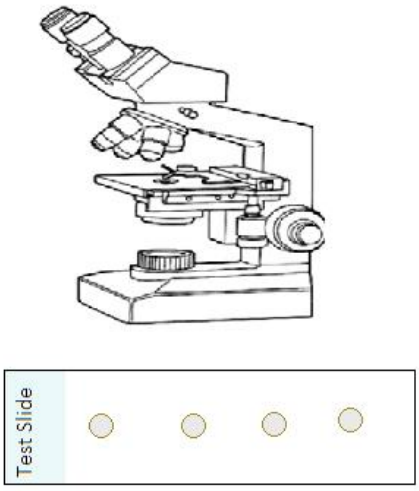

Figure 6: Checking of prepared LC based sensing platform using optical microscope.

3.2.3 Preparation of Cobalt Ferrite nanoparticles stabilized LC testing chamber

Prior to testing our sensor for arsenate detection, successful loading of cobalt ferrite ($CoFe_2O_4$) nanoparticles into the sensing platform was essential. For this, we needed to find optimal concentrations of both; Span 80 and $CoFe_2O_4$ nanoparticles, at which a stabilized and most efficient sensing platform was to be achieved. For all testing to follow, detecting solution comprised of; Span 80, varying v/v% of 1mM of $CoFe_2O_4$ and PBS as solvent. Sodium arsenate was our analyte solution. Each of the detecting solution had a total volume of 10ml. Figure 5 shows the schematic addition of solutions during these sensing experiments.

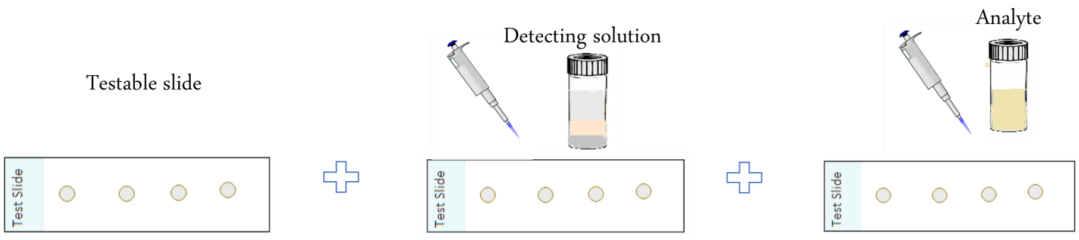

Figure 7: Schematic representation of sequence of addition of solutions while running LC based sensing experiments.

Optimizing Surfactant/Span 80 concentration

In order to establish the optimal concentration of Span 80 required to stabilize the sensing platform when loaded with nanoparticles, two series of tests were run, i.e. for a concentration of 0.01mM and 0.1mM of Span 80, while keeping all other conditions and variables similar.

Concentration of $CoFe_2O_4$ nanoparticles was varied for each Span 80 concentration until the first concentration of $CoFe_2O_4$ nanoparticles at which the system stability was achieved upon nanoparticles loading was established. All these tests were run for an analyte concentration of 100ppm of sodium arsenate. Each test was repeated at least thrice.

Optimizing cobalt ferrite nanoparticles concentration

After an optimal concentration of Span 80 was established at which sensing system achieved stabilization, tests were run to find the optimal concentration of $CoFe_2O_4$ at which the system showed best detection results for 100ppm of sodium arsenate. Each test was repeated at least thrice.

3.2.4 Testing varying concentration of Sodium Arsenate (1000ppm, 500ppm, 100ppm, 1ppm)

Once optimal concentrations of Span 80 and v/v% of 1mM of $CoFe_2O_4$ were established, tests were run to investigate detection of varying concentrations of sodium arsenate i.e. 1000ppm, 500ppm, 100ppm and 1ppm. Each test was repeated thrice.

3.2.5 Controls

Controls were run by testing each component; separately and in various combinations, on the testable 5CB-DMOAP activated slides in order to establish the behavior of each and confirm that the sensing was exclusively due to $CoFe_2O_4$ nanoparticles and sodium arsenate interaction only.

To run each control, an unused, partially aligned 5CB laden grid was used each time. The desired component(s) was (were) added to the grid using micropipette and

observations were noted and recorded using a polarized microscope. In table 3.2 below a sequential mention of controls performed is stated.

Table 2: List of controls performed

Sr No.	Component(s) Tested
1	Span 80
2	Phosphate buffer saline
3	Sodium Arsenate
4	$CoFe_2O_4$ nanoparticles
5	Span 80 and PBS solution mixture
6	Span 80, PBS, $CoFe_2O_4$ nanoparticles mixture solution
7	Span 80 and PBS solution mixture + Sodium Arsenate.

Note: In the last control foremost a drop from a solution of Span 80/PBS was added. Then, after a desired time (based on our results from running control #5), drop of Sodium Arsenate 100ppm was added.

Chapter 4. Results and Discussion

4.1 Cobalt ferrite nanoparticle synthesis & characterization

We have presented the synthesis of cobalt ferrite ($CoFe_2O_4$) nanoparticles by wet chemical method (co-precipitation) along with heat treatment at 500ºC. The advantage of this method over the others is that the control of production of ferrite particles, its size and size distribution is relatively easy and there was no need of extra mechanical or microwave heat treatment. The crystallite structure, size and morphology of the particles prepared by this method was studied by XRD and SEM.

4.1.1 XRD

The X-diffraction pattern (Fig.1) of the powder synthesized using this route shows that the final product is $CoFe_2O_4$. The sample showed reflection planes of (220), (311), (422), (511) and (440) which confirms the presence of cobalt ferrite and showed an almost 64% matching with JCPDS file No: 01-077-026

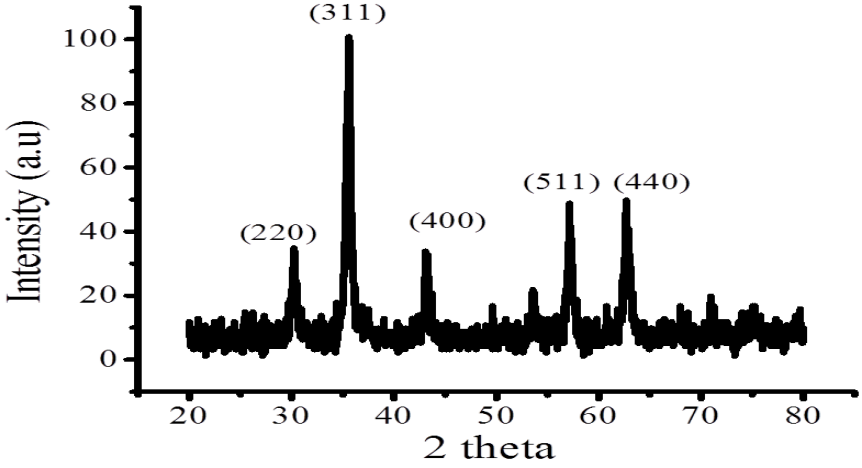

Figure 6: XRD graph of synthesized CoFe2O4 nanoparticles

4.1.2 SEM

The Scanning electron micrographs for synthesized cobalt ferrite nanoparticles were captured at varying magnifications of 70,000 and 100, 000, (See Fig8 and Fig 9 below) in order to assess particle morphology and distribution. Furthermore, for such small sized particles, no aggregation was noted in the images, which could be accounted for by the surfactant used i.e. CTAB, providing the needed stearic hindrance during synthesis. Finally, synthesized nanoparticles showed nearly spherical morphology as evident in Fig 9. The average particle size calculated was 21.3 ±2.8 nm.

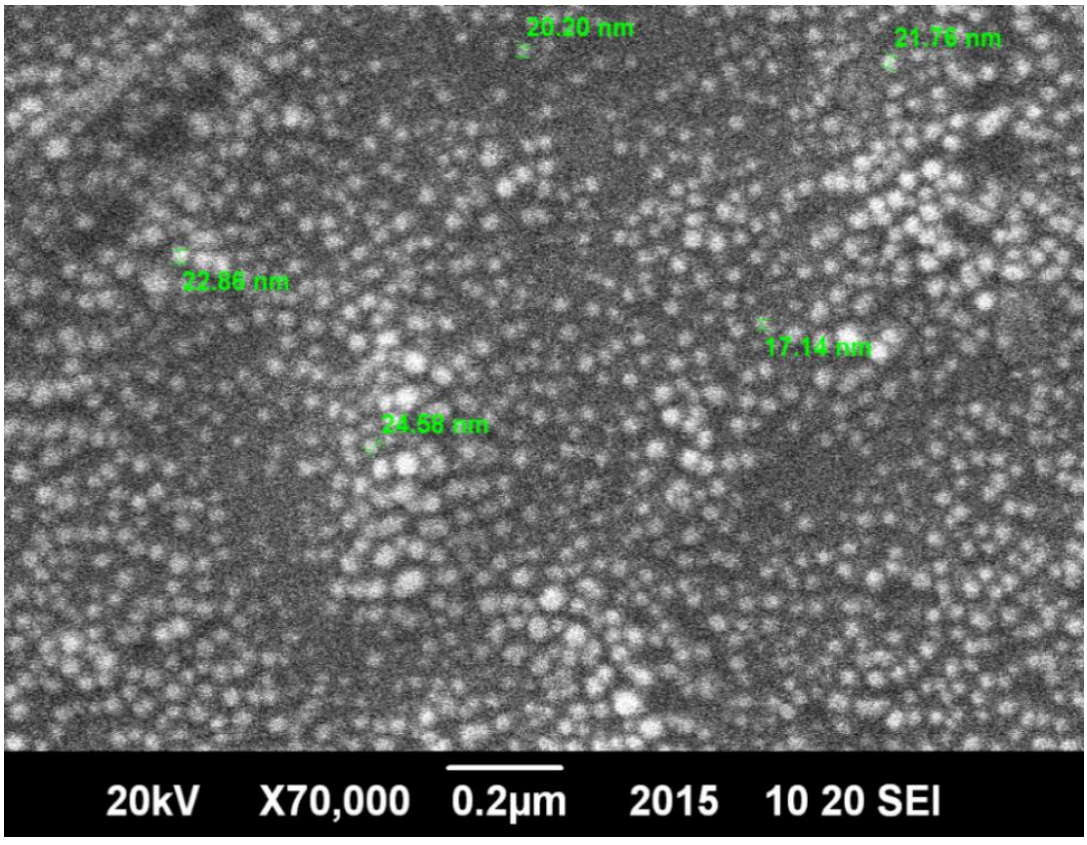

Figure 7: Scanning Electron micrograph of $CoFe_2O_4$ nanoparticles at a magnification of 70,000.

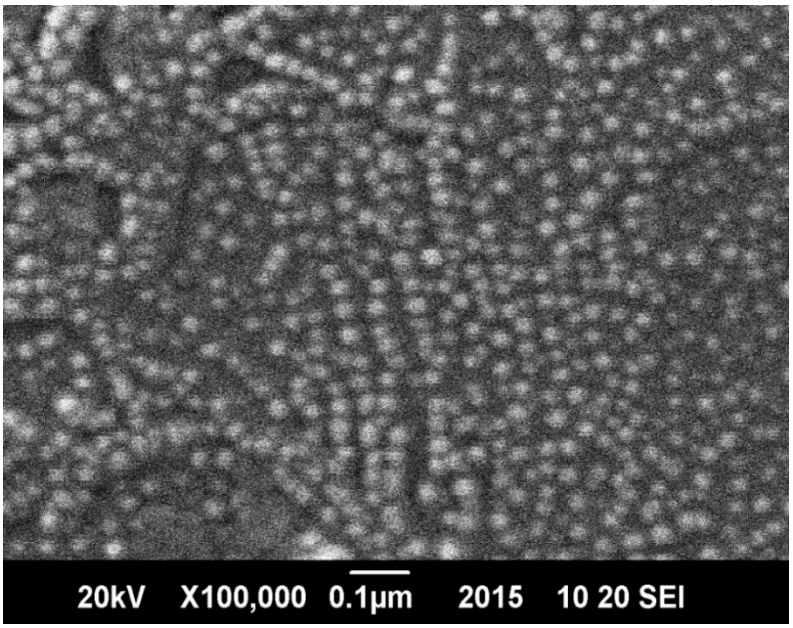

Figure 8: Scanning Electron micrograph of $CoFe_2O_4$ nanoparticles at a magnification of 100,000.

4.2 LC Based Optical Sensing

The synthesized nanoparticles were used as detecting molecules for sodium arsenate detection using liquid crystal as means of detection. Herein, physical disturbance expected as a result of reported adsorption of arsenate onto $CoFe_2O_4$ nanoparticles[15,51] was hypothesized to affect the already perturbation sensitive and optically anisotropic 5CB, resultantly expected to cause optically detectable response from an originally dark image (perpendicular 5CB alignment/light blockage) to a series of images with varying luminosity until a fully bright image (parallel alignment of 5CB/complete light leakage) is observed when viewed over a course of time under polarized microscope. However, in order to test this hypothesis, the foremost step was preparing of an optical LC based sensing platform.

4.2.1 Preparation of Optical LC Based Sensing Platform

Preparation of optical LC based sensing platform was governed by the choice of substrate used for LC alignment. In this study, microscopic glass (borosilicate) slides,

already widely used substrate for LC based sensing, were chosen as the bottom substrate due to their stable, robust nature along with easy availability [38]. Subsequently, the steps involved in prepping optical sensing platform included the reported procedure of; glass slide cleaning and activation, followed by confinement of LC within gold grids along with their annealing and finally checking these slides for further usage for sensing purposes [50].

In LC based sensing studies, for each test, images of a minimum of 4 grid cells/chambers within an entire grid mesh are captured over the needed time period [45, 46, 47]. Below in Fig11 are the results of confined and annealed 5CB within gold grids for varying conditions.

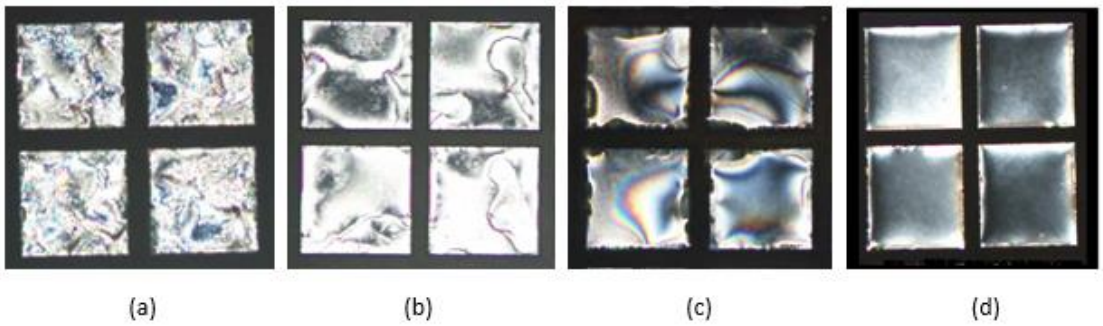

Figure 9: Optical images of 5CB confined and annealed in TEM grids under polarized microscope when a) no slide washing or DMOAP activation, b) slide washing was done but no DMOAP slide activation c) Washed and DMOAP activated slide with poor alignment d) Washed and DMOAP activated slide with proper degree of partial alignment.

From the images above, Fig 10 a) and b), it is evident that stringent cleaning of slides using a powerful oxidizing agent i.e. Piranha, along with slide activation using DMOAP is critical while prepping optical sensing platform. In each of these we noted that 5CB was not able to align. These results show agreement with other studies which reported the need for cleaning and activation of slides prior to annealing and further usage [39]. This is attributed to the fact that DMOAP has octadecyl hydrocarbons chains ($C_{18}H_{37}$) which perpendicularly align LC, thus showing dark texture between cross polarizer [40]. Without these anchoring agents, LC molecules cannot orient perpendicularly and hence no proper alignment has been found as shown in Fig 10a) While Piranha cleaning helped in uniform deposition of silane layer. This silanization layer on glass substrate also contributes to the uniform anchorage of LCs molecules.

Furthermore, Fig 10c) and fig 10 d) show the; poorly-partially aligned and properly-partially aligned 5CB on cleaned and DMOAP activated slides, respectively. While prepping of sensing platform throughout this study, after cleaning and activation of slides followed by confining and annealing of 5CB within the grids on these slides, they were tested under polarized microscope. Subsequently, the grids which showed poor partial alignment (like Fig 10c) were rejected manually while those that showed proper partial alignment (like Fig 10d), were regarded as testable grids, fit for further sensing purposes.

4.2.3 Preparation of Cobalt Ferrite Nanoparticles Stabilized LC Testing Platform

Once optical sensing platform was successfully fabricated, the next step was to use it for our desired sensing i.e. detection of sodium arsenate using cobalt ferrite nanoparticles. Based on existing literature, combining principles of basic sensor along with LC based sensing in particular, the scheme of testing was foremost set. This meant that since optical LC based sensing is based on the optical transition from dark (completely blocked light/perpendicular alignment) to bright (complete light leakage/parallel alignment) or vice versa, it was important to start with 5CB completely aligned in one direction. As explained in Chapter 2, substrate aligning agent like DMOAP results in partial perpendicular alignment of LC. While for aqueous-air interface alignment a surfactant is used, resulting in complete alignment of LC. However, as a basic sensor principle it is desirous that at this point our receptor or detecting molecules (cobalt ferrite nanoparticles as in our case), are successfully embedded in the system such to give us a stable, completely aligned 5CB system, in order for the analyte alone to bring about the desired optical response. Resultantly, to partially aligned 5CB grids we added not only surfactant but detecting molecules as well at this stage in the form of a mixed solution. This was done to experience not only the usual effect a surfactant has on LC alignment but also to allow detecting molecule to successfully embed with the LC resulting in a stabilized LC sensing chamber, with fully aligned LC prior to addition of analyte.

Our detecting solution comprised of cobalt ferrite nanoparticles as detecting molecules with Span 80 selected as our surfactant of choice while PBS was used as our solvent. Span 80, is relatively a fresh entrant in the list of used surfactants for complete LC alignment in sensing. Largely lipids have been reported as surfactants [52] however they have their limitation of requiring tedious processing for usage. Subsequently, as recently suggested by Zakir and colleagues, Span 80 was used for its convenient processing and LC stabilizing features. Furthermore, PBS was used as our choice of solvent since water was observed to interfere with LC, presenting its own set of rainbow like patterns and so PBS solvent has been used and pH of the system was maintained to 7 using this solvent. It helps to identify better detection patterns than in previous case

In order to successfully embed cobalt ferrite nanoparticles, we needed to find optimal concentrations of both; Span 80 and cobalt ferrite nanoparticles, at which a stabilized and most efficient sensing platform was to be achieved. Results obtained are mentioned in the sections to follow.

Optimizing Surfactant/Span 80 Concentration

Based on the report by Zakir *et al.*, wherein Span 80 has shown alignment of 5CB for a concentration range of 0.01mM to 0.1mM, we foremost ran two series of tests, i.e. for a concentration of 0.01mM and 0.1mM of Span 80, while keeping all other conditions and variables similar. $CoFe_2O_4$ nanoparticles concentration was varied for each series, until the first concentration was achieved at which stabilized system was noted. All these tests were run for an analyte concentration of 100 ppm of sodium arsenate.

In Fig 11 below are the results obtained for a Span 80 concentration of 0.01mM with varying $CoFe_2O_4$ nanoparticles v/v% concentrations.

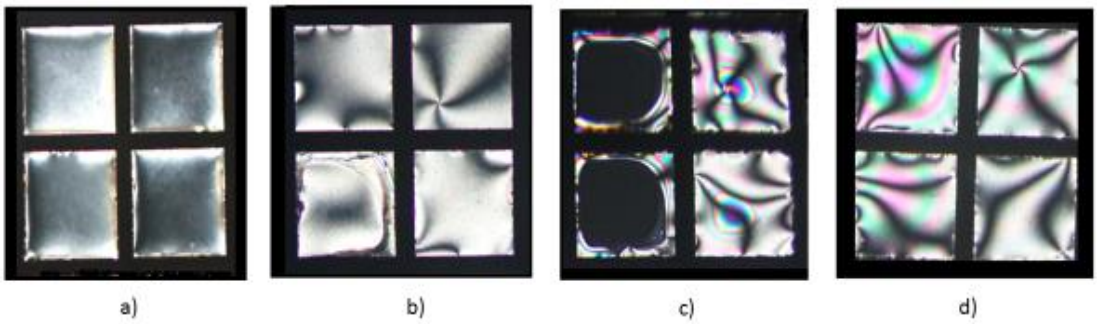

Figure 10: Optical images obtained for testing performed to achieve stable loading of $CoFe_2O_4$ nanoparticles using a Span 80 concentration of 0.01mM a) partially aligned 5CB prior to testing each detection solution with varying v/v% of 1mMof $CoFe_2O_4$ b) Immediately after adding 15% v/v $CoFe_2O_4$/Span 80 0.01mM/PBS, c) Immediately after adding 10% v/v $CoFe_2O_4$/Span 80 0.01mM/PBS, d) Immediately after adding 5% v/v $CoFe_2O_4$/Span 80 0.01mM/PBS

The optical images in Fig11 b), c) and d) reveal the effect of loading 15%, 10% and 5% v/v of $CoFe_2O_4$/Span 80 0.01mM/PBS solutions, respectively. At the addition of each of the varying v/v% concentration of 15, 10 and 5% it was noted that buffering, buffering along with bursting of LC and buffering was experienced, respectively. Subsequently, these tests revealed that at these concentrations no further analyte detection was possible since the originally partially aligned 5CB laden grids showed no stable, homeotropic alignment of LC upon addition of the detecting solution with 0.01mM of Span 80 concertation. So, it was concluded that Span 80 concentration of 0.01mM was not appropriate for successful loading of cobalt ferrite nanoparticles such as to result in stable, fully aligned LC.

Resultantly, we followed this with another series of tests, this time for a Span 80 concentration of 0.1mM. The results obtained are given below in Fig 12.

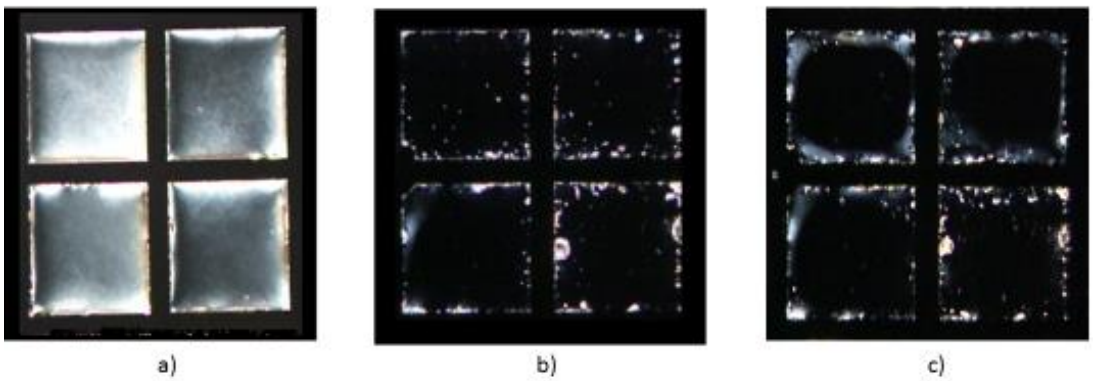

Figure 11: Optical images obtained for testing performed to achieve stable loading of $CoFe_2O_4$ nanoparticles using a Span 80 concentration of 0.1mM; a) partially aligned 5CB prior to testing b) Immediately after adding drop of detecting solution consisting of 15% v/v $CoFe_2O_4$/Span 80 0.1mM/PBS, c) Immediately after adding drop of 100ppm of sodium arsenate

Testing revealed that for a concentration of 0.1mM of Span 80, homeotropic alignment was noted for a detection solution comprising of 15% v/v of 1mM of $CoFe_2O_4$ nanoparticles. Results above show the clear transition from partially aligned 5CB (Fig 12a) towards a dark image (Fig 12b) upon addition of mentioned composition of detecting solution, hinting at successful loading of nanoparticles within the LC sensing platform. Few important findings were established from these results.

Foremost, that almost 75% of successful loading was achieved since 3 out of 4 grid cells/chambers showed stable LC (bursting was observed in one of the 4 grid cell/chambers). This, when followed with addition of a drop of 100ppm of sodium arsenate (Fig 12c) revealed that all 4of these grid cells/chambers experienced bursting of LC. In order to further cement these results, the tests were repeated thrice. Results of which are given in Fig13 below.

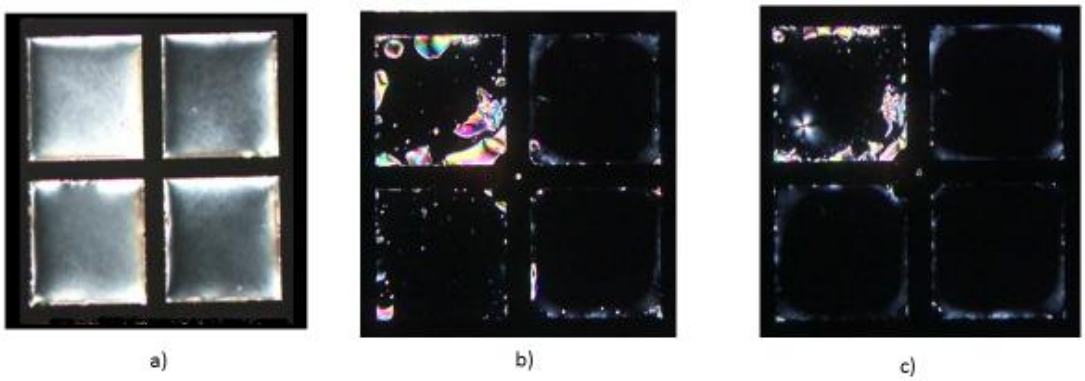

Figure 12 Optical images obtained for testing performed for a detecting solution consisting of 15% v/v of $CoFe_2O_4$/Span 80 0.1mM/PBS when tested against 100 ppm of sodium arsenate (analyte solution) a) partially aligned 5CB prior to testing b) Immediately after adding drop of detecting solution, c) Immediately after adding a drop of analyte solution

Upon repeating the tests, it was observed that the success ratio of stabilization of LC sensing chamber at this concentration of $CoFe_2O_4$ nanoparticles to not aligning successfully was 1:3. As shown above partially aligned 5CB (Fig 13a) showed bursting of LC in 2 of the 4 chambers (Fig 13b) while after adding analyte solution further bursting of LC was seen (Fig 14c). Subsequently, it was concluded that 15% of 1mM of $CoFe_2O_4$ nanoparticle solution was still very concentrated to allow sufficient stabilization of LC chambers. This indicated that for further testing lower v/v% concentrations of 1mM of $CoFe_2O_4$ nanoparticles within our detecting solution should be chosen.

Another important observation was that although complete homeotropic alignment was achieved, some very tiny patterns had appeared after addition of this detecting solution suggesting the need to explore the cause behind such an occurrence.

Optimizing v/v% Concentration of Cobalt Ferrite nanoparticles

Below are the results obtained for varying v/v% concentration of 1mM of $CoFe_2O_4$ nanoparticles using a Span 80 concentration of 0.1mM.

Foremost, gathering from the results observed for 15 v/v% of 1mM of $CoFe_2O_4$ nanoparticles/0.1mM Span 80/PBS solution, further testing was done by going down the concentration gradient wherein tests were run for 10 v/v% of $CoFe_2O_4$

nanoparticles/0.1MM Span 80/PBS solution. Results from repeated testing are given in Fig15 below.

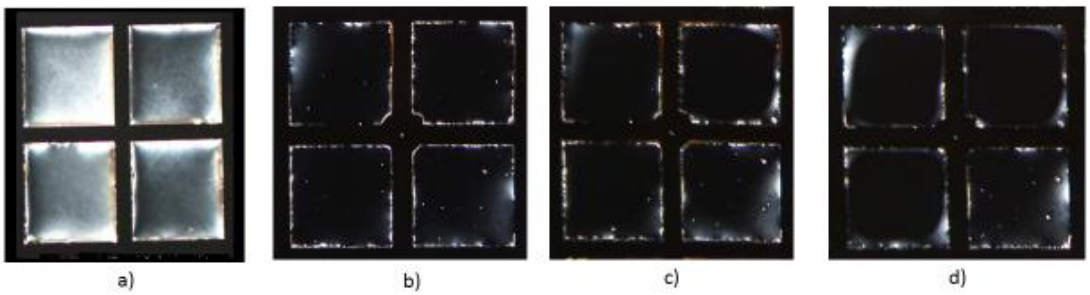

Figure 13: Optical images obtained for testing performed for a detecting solution consisting of 10% v/v of $CoFe_2O_4$/Span 80 0.1mM/PBS when tested against 100 ppm of sodium arsenate (analyte solution) a) partially aligned 5CB prior to testing b) Immediately after adding drop of detecting solution, c) Immediately after adding a drop of analyte solution

Testing at this concentration revealed that unlike detecting solution having 15 v/v% of 1mM of $CoFe_2O_4$ nanoparticles, detecting solution with 10% v/v% of 1mM of $CoFe_2O_4$ nanoparticles did not show immediate bursting of LC after addition of detecting solution (Fig 14b). Moreover, bursting of LC was seen after 100ppm of sodium arsenate addition and that too was later than that observed at 15% (Fig 14c and 14d). So a trend was observed that at lower concentration, bursting of LC both decreased and delayed. Resultantly, experimentations to follow were done using further lower v/v% concentrations of 1mM of $CoFe_2O_4$ nanoparticles.

After 10% tests were run for detecting solution with 5 v/v% concentration of 1mM of $CoFe_2O_4$nanoparticles. Fig 15 below shows the results obtained.

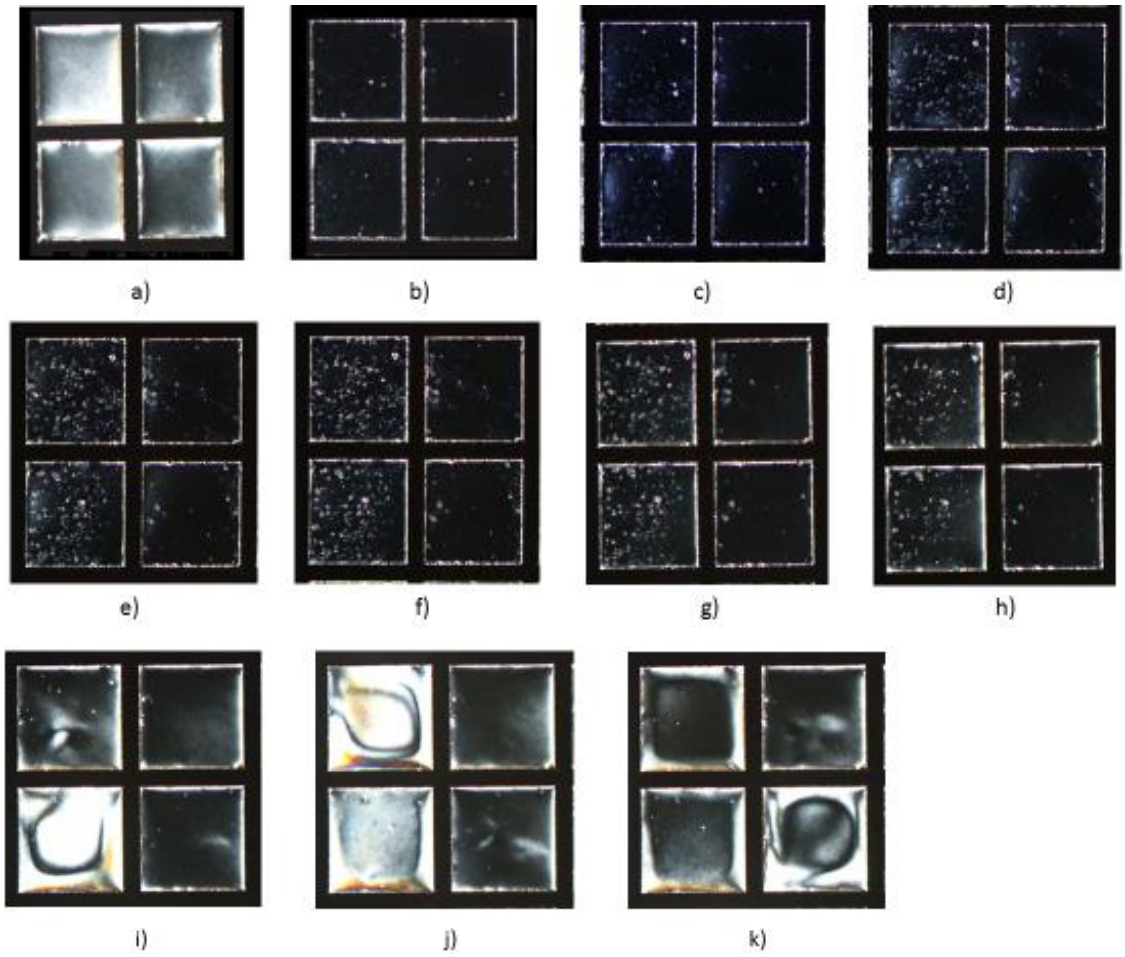

Figure 14: Optical images for testing performed for a detecting solution consisting of 5% v/v of $CoFe_2O_4$/Span 80 0.1mM/PBS when tested against 100 ppm of sodium arsenate (analyte solution) a) partially aligned 5CB prior to testing b) Immediately after adding drop of detecting solution, c) Immediately after adding drop of analyte solution d) 10 minutes after , e) 20minutes after, f) 30minutes after, g) 40minutes after, h) 46 minutes after, i) 47 minutes after, j) 47 minutes after, k) 48 minutes after addition of analyte solution.

It was noted for the first time that not only successful loading of nanoparticles was achieved after addition of detecting solution (Fig 56b) but that following it with addition of analyte solution (Fig 15c) also resulted in stable LC chambers and a series of observations were made. It was noted foremost, that tiny patterns were observed (Fig 15 d, e, f, g, h) until after 46 minutes the LC started showing signs of planar alignment (Fig 15 i and j) represented by the brightness noted, after which the LC again realigned homeotropically (Fig 15j) due to the presence of both DMOAP and surfactant. Repeating the test thrice, average detection time (time since addition of addition of

analyte solution till the time it takes for LC to realign once again homeotropically) was 42minutes. These results indicated the need to establish optimal v/v% concentration of 1mM of $CoFe_2O_4$nanoparticles by going both up and down 5% concentration.

Resultantly, foremost tests were run for a detecting solution comprising 2.5 v/v% concentration of 1mm of $CoFe_2O_4$nanoparticles. Results are given below in Fig 16.

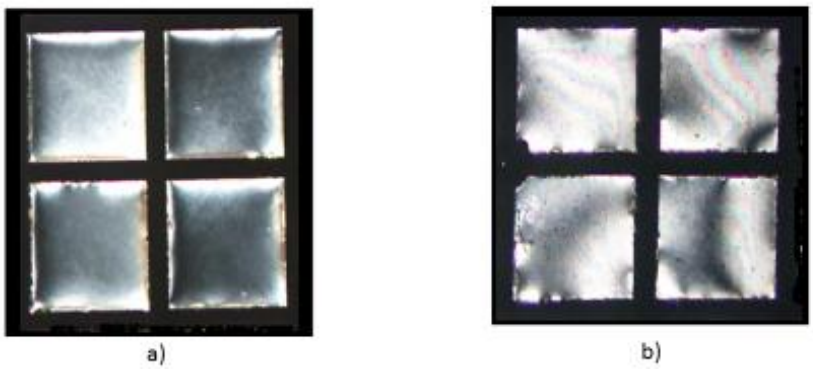

Figure 15: Optical images for testing performed for a detecting solution consisting of 2.5% v/v of $CoFe_2O_4$ /Span 80 0.1mM/PBS when tested against 100 ppm of sodium arsenate (analyte solution) a) partially aligned 5CB prior to testing b) Immediately after adding drop of detecting solution

Results in Fig 16 revealed that after addition of detecting solution with 2.5 v/v% concentration of 1mM of $CoFe_2O_4$nanoparticles, buffering was observed repeatedly and so it was concluded that this concentration was not appropriate for loading of nanoparticles and stabilizing of LC.

Subsequently, as stated earlier, after going down the 5 v/v% concentration of 1mM of $CoFe_2O_4$nanoparticles, a series of tests were further conducted for detecting solution having 7 v/v% concentration of 1mM of $CoFe_2O_4$ nanoparticles. Results are given in Fig 17 below.

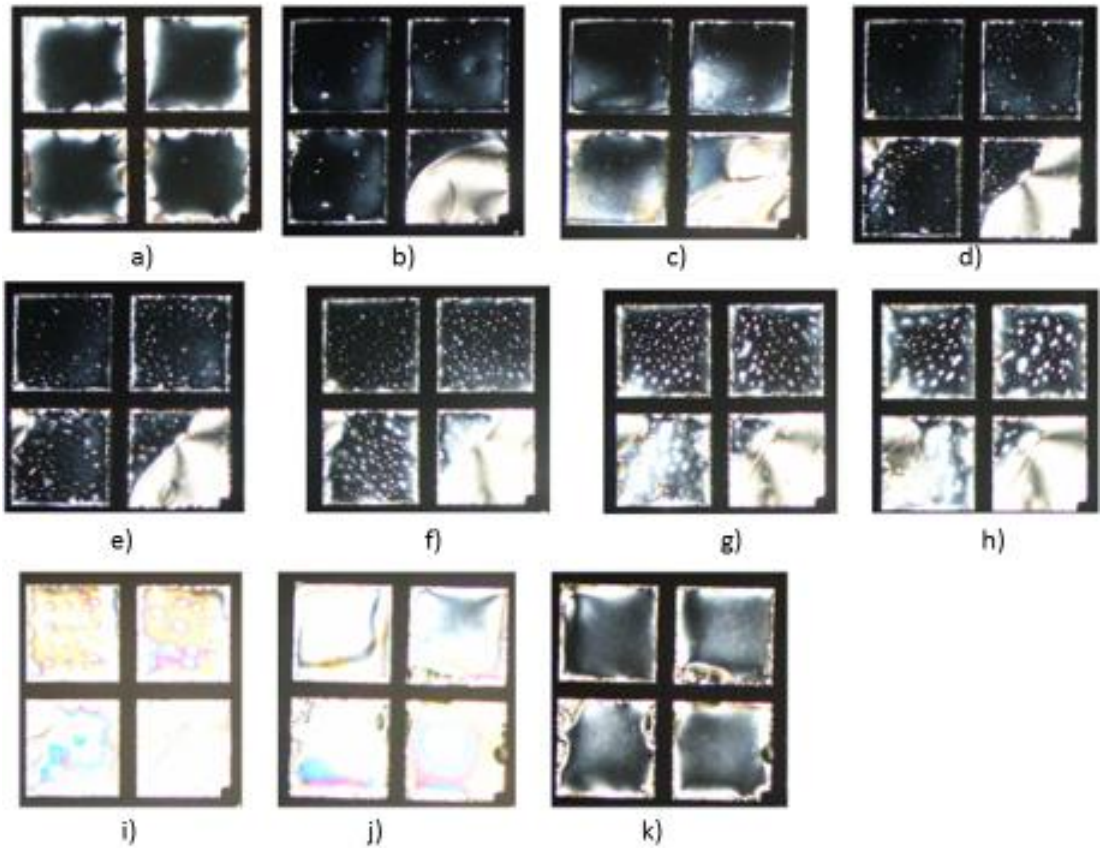

Figure 16: Optical images for testing performed for a detecting solution consisting of 7% v/v of $CoFe_2O_4$ /Span 80 0.1mM/PBS when tested against 100 ppm of sodium arsenate (analyte solution) a) partially aligned 5CB prior to testing b) Immediately after adding drop of detecting solution c) Immediately after adding drop of analyte solution d) 5 minutes after , e) 10minutes after, f) 15minutes after, g) 20minutes after, h) 25 minutes after, i) 28 minutes after, j) 30 minutes after, k) 31 minutes after addition of analyte solution.

Results from repeated testing with detecting solution comprising of 7% v/v of 1mM of $CoFe_2O_4$ nanoparticles in Fig 17 revealed a set of findings. Foremost, it was noted that for this composition of detecting solution successful stabilization was achieved after its addition(Fig 17b showing homeotropic alignment) and that this stability extended even after addition of analyte solution (Fig 17c). Furthermore, patterns were detected (Fig 17 d and e) (as were also seen in case of detecting solution comprising of 5% v/v of 1mm of $CoFe_2O_4$ nanoparticles) however these patterns were more stronger and distinct than those seen in case of detecting solution comprising of 5% v/v of 1mm of $CoFe_2O_4$ nanoparticles. Moreover, with passage of time the initially slight patterns grew more distinct and luminosity within chambers also increased (Fig

17 e, f, g and h) until eventually planar state (Fig 17 i and j) was observed after which the LC realigned again and a stable system was re-established (Fig 17 k). Repeating these tests thrice revealed the average detection time to be 28minutes.

Finally, gathering from analyzing and comparing the results obtained from varying v/v% concentrations of 1mM of $CoFe_2O_4$ nanoparticles, a series of conclusions were drawn. Table 3 below lists the various notable findings and trends observed.

It is evident from table below that for higher concentrations (15 and 10%) of v/v% of 1mM of $CoFe_2O_4$ nanoparticles, completely successful loading of nanoparticles and LC stabilization was not achieved rather bursting and buffering were more prominent. This can be attributed to the explanation that a Span 80 concentration of 0.1mM was not enough to sufficiently load nanoparticles while stabilizing the system such as to achieve complete homeotropic alignment. However, this buffering and bursting decreased by decreasing the cobalt ferrite v/v% concentration within detecting solution until stability was seen for concentrations of 7and 5% v/v of 1mM of $CoFe_2O_4$ nanoparticles. While going further below 5% v/v of 1mM of $CoFe_2O_4$ again showed no stability at all. These results suggested that optimal concentration of v/v% of 1mM of $CoFe_2O_4$ nanoparticles was between 10 and 5%. Gauging from results best detection time was seen for 7% along with a prominent display of pattern formation along with least detection time, making it the optimal concentration.

Table 3: Results for varying v/v% concentration of $CoFe_2O_4$ nanoparticles for fixed Span 80 concentration of 0.1mM against 100ppm Sodium Arsenate

$CoFe_2O_4$ concentration	**Observations**	**Detection times**	**Number of test repeats**
15%	Mostly LC bursting	36 min	x3
10%	LC bursting, buffering, patterning	39 min	x3
7%	LC stabilization, Prominent pattern	28 min	x3
5%	LC stabilization, less prominent pattern, Buffering	42 min	x3
2.5%	Buffering	none	x3

4.2.3 Testing varying concentrations of Sodium Arsenate (1000ppm, 500ppm, 100ppm, 1ppm)

Once the optimal concentrations of Span 80 and v/v% of $CoFe_2O_4$ nanoparticles were established, testing was performed for varying sodium arsenate concentrations. Experimentation revealed that scheme of events was similar for all test runs i.e., homeotropic alignment and pattern appearance upon addition of detecting solution followed by growing of these patterns after addition of analyte solution, with luminosity within chambers/cells increasing until planar alignment was finally observed followed with re-stabilization of LC to original state. However, once again series of varying trends were noted for the varying sodium arsenate concentrations. The results are explained below in fig 18.

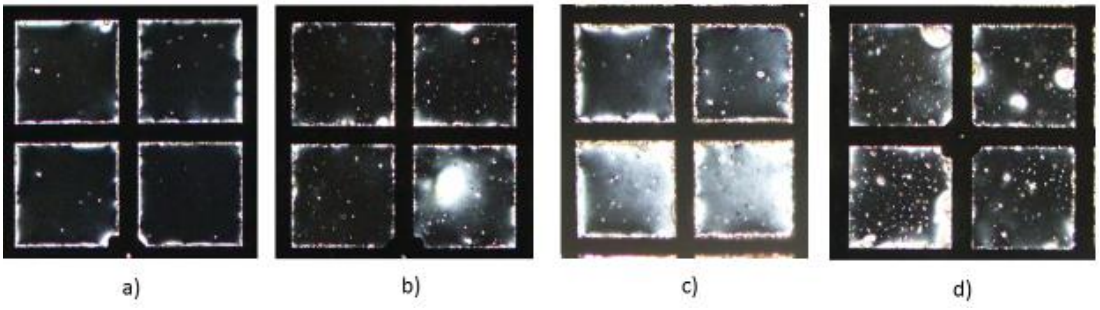

Figure 17 Pattern trends observed for varying Sodium Arsenate concentration; a) 15 min after addition of 1000ppm of sodium arsenate, b) 15 min after addition of 500ppm of sodium arsenate, c) 15 min after addition of 100ppm of sodium arsenate, d) 15 min after addition of 1ppm of sodium arsenate

Foremost, a varying trend in pattern formation was noted as shown in Fig 18. It was observed that as we moved down the concentration gradient i.e. from 1000 to 1 ppm of sodium arsenate, pattern size increased, with small patterns for higher concentrations (Fig 18 a and b) while larger patterns were observed for lower concentrations (fig 18 c and d). This very important observation led to two important conclusions. First, that as already stated in previous section, patterns started appearing as soon as detecting solution was added which suggested that since Span 80 or PBS are not reported to be responsible for creating patterns so patterns were due to the third component i.e. the heavy nanoparticles. This explanation stands in accord with an

already reported study that studied the behavior of adding of nanoparticles within LC system. Here it was concluded that nanoparticles create defect sites in LC [53]. Subsequently, these defect sites created by nanoparticles (that appeared after addition of detecting solution) when viewed under polarized microscope appeared as patterns. And so pattern formation in itself cannot be a mark of presence/detection of sodium arsenate. Also, all tests revealed that the scheme shown during each experiment was same i.e. homeotropic alignment and pattern appearance upon addition of detecting solution followed with growing of these patterns after addition of analyte solution, with luminosity of chambers increasing until finally planar alignment was observed followed with re-stabilization of LC to original state. And so this too was associated with the dynamics between LC and nanoparticles and can be justified with the following explanation i.e. upon addition of nanoparticles based detecting solution, homeotropic alignment although is achieved courtesy to sufficient surfactant concentration, these nanoparticles being heavy create defect sites upon interaction with LC. With growing time this intercalation of the two materials grows more resulting in more stronger patterns along with disruption of LC, resulting in increased luminosity until finally the LC are completely planar (parallel wrt substrate)resulting in complete light leakage and so a bright image is observed. Eventually the LC system as per rules of equilibrium shifts back to its stable state and so once again a partially aligned state of LC is noted. However, it is the results seen in fig 18 that establish that sodium arsenate addition too has an effect which explains its presence and is a marker of its detection. The change in pattern intensity reveals that arsenate is not responsible for creating patterns rather it affects the intensity of patterns with slight patterns at higher analyte concentration while larger patterns at lower concentrations. Moreover, these observations can also be explained by the reasoning that at higher analyte concentrations there is more sodium arsenate which when binds with nanoparticles results in not allowing as prominent defect sites (i.e. patterns) as those created when analyte concentration was lower meaning less arsenate to bind to nanoparticles allowing it to freely cause larger defect sites.

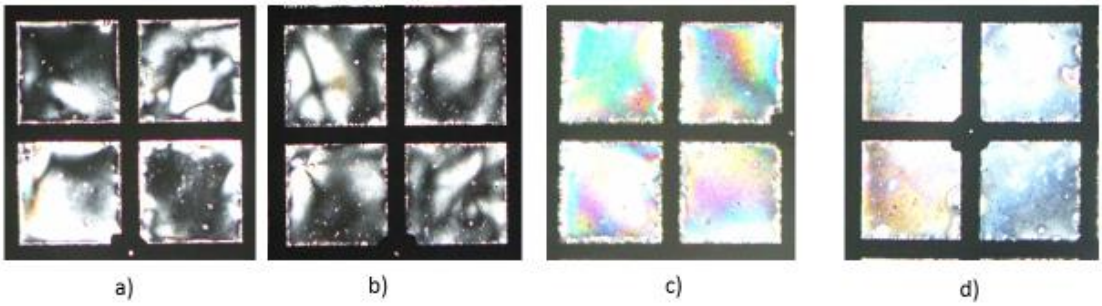

Figure 18 Transition trends observed for varying Sodium Arsenate concentration; a) for 1000ppm of sodium arsenate, b) for 500ppm of sodium arsenate, c) for 100ppm of sodium arsenate, d) for 1ppm of sodium arsenate

Furthermore, varying trend was also observed during the transition phase i.e from homeotropic to planar alignment. It was noted that at higher analyte concentration no rainbow patterning was observed (Fig 19a and b) while for lower concentrations, pronounced rainbow patterns were seen (Fig 19c and d) right before planar alignment was achieved. These results reveal that rainbow patterns, which have been typical of water, are seen in lower analyte concentrations since they are dilute with less of sodium arsenate and subsequently since higher analyte concentrations had less water and more sodium arsenate so no rainbow patterns were seen.

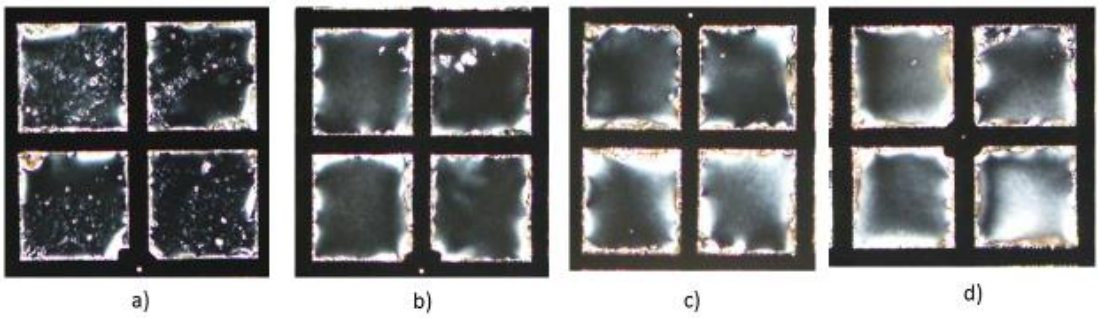

Figure 19 Clearance trends observed for varying Sodium Arsenate concentration; a) for 1000ppm of sodium arsenate, b) for 500ppm of sodium arsenate, c) for 100ppm of sodium arsenate, d) for 1ppm of sodium arsenate

Finally, for varying sodium arsenate concentrations, a varying trend was noted in clearance as well i.e. once the LC re-achieved their stable state i.e. partially aligned,

for higher analyte concentration complete clearance was not seen (Fig 20 a) while for lower concentrations the 5CB returned to its original state showing a clear image with no residue left (Fig 20 b, c and d). This observation reveals that at higher analyte concentration the sodium arsenate is so much that even after realignment to homeotropic state the sodium arsenate does not let nanoparticles clear away.

Finally, table 4 below summarizes the varying trends observed at varying analyte concentrations. Though all trends have already been discussed above, the detection time of sensing has not been discussed. From the table it is evident that no pronounce/significant change in detection time is noted for varying analyte concentration. However, that is a very significant finding since it reveals that sensing time is affected by nanoparticles and not sodium arsenate.

Table 4: Trends obtained for varying concentrations of Sodium Arsenate

Arsenate conc. (ppm)	**Pattern trends**	**Transition trends**	**Clearance trends**	**Time (/min)**
1000	Small, less patterns	No rainbow transitions	No clearance	31
500	Small, less patterns	No rainbow transitions	Cleared	27
100	Larger, more patterns	Rainbow transitions	Cleared	28
1ppm	Large, More patterns	No rainbow transitions	Cleared	29

4.2.4 Controls

Controls were run in order to confirm that the sensing was exclusively due to $CoFe_2O_4$ nanoparticles and sodium arsenate interaction only. The results are shown in figure22.

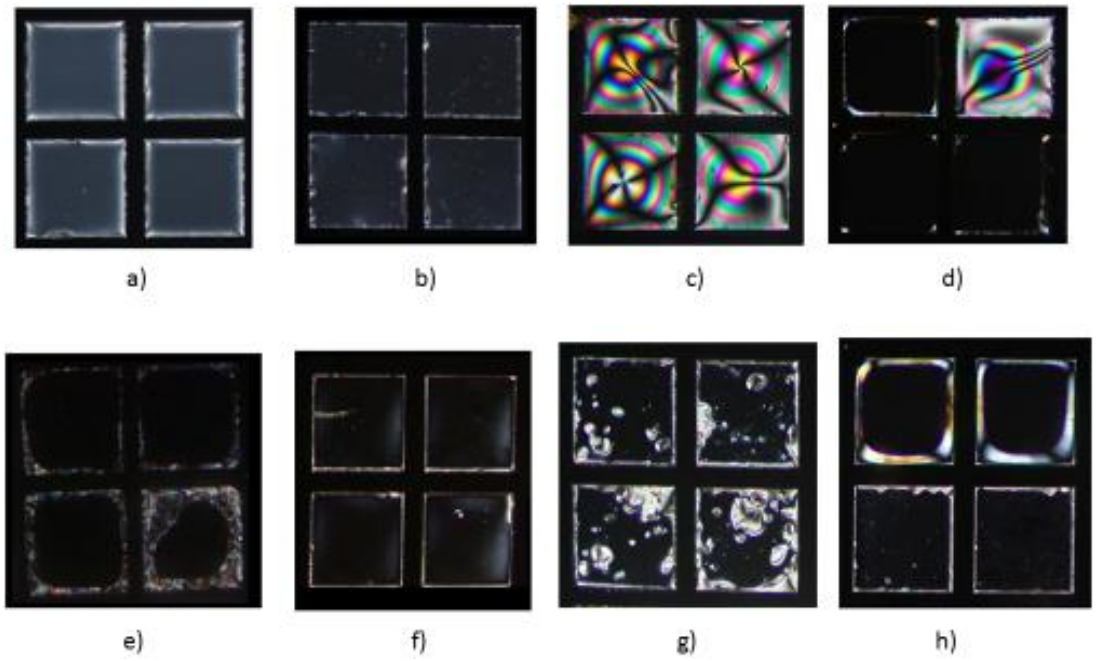

Figure 20 Optical images obtained for controls a) representative image of partially aligned 5CB prior to testing each component or combination of components b) after adding Span 80 0.1mM, c) after adding PBS, d) after adding 100ppm of sodium arsenate, e) after adding $CoFe_2O_4$ nanoparticles, f) after adding Span 80 0.1Mm/PBS, g) after adding $CoFe_2O_4$/Span 80 0.1mM/PBS, h) after adding Span 80 0.1mM/PBS followed by drop of 100ppm of sodium arsenate.

Figure 21 reveals the results observed upon addition of each component and combination of components when added separately to partially aligned 5CB (Fig 21 a). When Span 80 of 0.1mM concentration was added to partially aligned 5CB it resulted in complete alignment of 5CB represented by a dark image, a result which stands in accordance with the already reported [53] effect surfactants have on partially aligned 5CB(Fig 22b). Next, PBS addition to LC showed the already reported typical buffered rainbowing patterns (Fig 21c) while addition of 100ppm sodium arsenate (Fig 21d) as well as cobalt ferrite nanoparticle solution (Fig 21 e) to partially aligned 5CB resulted in bursting of LC. This not only revealed that solutions of these were too strong for the sensitive LC but also that in case of cobalt ferrite nanoparticles, surfactant played a critical role in stably embedding nanoparticles within 5CB. Furthermore, addition of Span 80/PBS gave the as expected result of complete homeotropic alignment as seen in

Fig 21 f) and confirmed further that Span 80 was responsible for complete alignment and that PBS in combination did not result in any patterns. Finally the two most important controls to confirm our findings included foremost adding a combination of Span 80/PBS/$CoFe_2O_4$ nanoparticles to partially aligned 5CB and note the observations. It was noted that large defect site or patterns were created (Fig 21g) and since none appeared in Fig 21b) or 21 f) so it is confirmed that nanoparticles alone are responsible for defect sites/patterns. Also, these patterns showed a similar scheme that is of appearing, growing larger, luminosity increasing until planar alignment followed with shifting of system back to its equilibrium state i.e. partially aligned 5CB and so confirms that this scheme of events is due to nanoparticle and LC interaction. Finally, to partially aligned 5CB Span 80/PBS was again added which resulted in image as seen in fig 21 f) however to this sodium arsenate 100ppm was added and it was seen that it resulted in bursting of LC. This confirmed, that sodium arsenate when added alone to 5CB system having Span 80/PBS did not result in the observations seen during sensing of analyte using detecting solution.

Chapter 5. Conclusions and Future Directions

This research effort concludes successful sensing of sodium arsenate based on the reported adsorption affinity it has for cobalt ferrite ($CoFe_2O_4$) nanoparticles, using the perturbation sensitive and optically anisotropic liquid crystals (LC), as medium of detection. Foremost, the challenge to load and stably embed the synthesized nanoparticles within the prepped LC sensing platform was achieved. This was accomplished by investigating and establishing the optimal concentrations of both; surfactant i.e. Span 80 followed by the varying v/v% concentrations of 1mM of $CoFe_2O_4$ nanoparticles. Finally, upon testing this sensing platform for sodium arsenate detection, it was revealed that our cue for arsenate-nanoparticle interaction was the optically distinguishable effect arsenate presence had on the nanoparticle-LC created defect sites that appeared as patterns under polarized microscope. Significantly, for varying arsenate concentrations (1000ppm, 500ppm, 100ppn and 1ppm) discernable trends were observed, showing promise of not only establishing a sensor with sensitivity for these concentrations but also a potential to detect further trace amounts. Lastly, a very important conclusion we arrived at from this investigation was that the detection time was influenced largely by the nanoparticles.

This resultantly sets the possible trajectory for future exploration. Herein, foremost the nanoparticles can be targeted for both; quicker detection along with improved detection/sensitivity by means of exploiting the size and/or morphology as well as magnetic potential of cobalt ferrite nanoparticles within liquid crystals. Furthermore, selectivity of these particles towards other arsenic and other heavy metal species can be manipulated to advantage by surface modification and functionalization.

Chapter 6. References

[1] Brammer, H., and Ravenscroft, P. (2009). Arsenic in groundwater: a threat to sustainable agriculture in South and South-east Asia. *Environment International*, *35*(3), 647-654.

[2] Choong, T. S., Chuah, T. G., Robiah, Y., Koay, F. G., and Azni, I. (2007). Arsenic toxicity, health hazards and removal techniques from water: an overview. *Desalination*, *217*(1), 139-166.

[3] Melamed, D. (2005). Monitoring arsenic in the environment: a review of science and technologies with the potential for field measurements. *Analytica Chimica Acta*, *532*(1), 1-13.

[4] Shibaev, P. V., Wenzlick, M., Murray, J., Tantillo, A., and Howard-Jennings, J. (2015). Rebirth of Liquid Crystals for Sensoric Applications: Environmental and Gas Sensors. *Advances in Condensed Matter Physics*, *2015*.

[5] Sivakumar, S., Wark, K. L., Gupta, J. K., Abbott, N. L., and Caruso, F. (2009). Liquid crystal emulsions as the basis of biological sensors for the optical detection of bacteria and viruses. *Advanced Functional Materials*, *19*(14), 2260-2265.

[6] Li, G., Gao, B., Yang, M., Chen, L. C., and Xiong, X. L. (2015). Homeotropic orientation behavior of nematic liquid crystals induced by copper ions.*Colloids and Surfaces B: Biointerfaces*, *130*, 287-291.

[7] Wang, P. H., Yu, J. H., Zhao, Y. B., Li, Z. J., and Li, G. Q. (2011). A novel liquid crystal-based sensor for the real-time identification of organophosphonate vapors. *Sensors and Actuators B: Chemical*, *160*(1), 929-935.

[8] Ding, X., and Yang, K. L. (2012). Liquid crystal based optical sensor for detection of vaporous butylamine in air. *Sensors and Actuators B: Chemical*,*173*, 607-613.

[9] Zhang, M., and Jang, C. H. (2013). Liquid crystal based optical sensor for imaging trypsin activity at interfaces between aqueous phases and thermotropic liquid crystals. *Bulletin of the Korean Chemical Society*, *34*(10), 2973-2977.

[10] Hu, Q. Z., and Jang, C. H. (2012). A simple strategy to monitor lipase activity using liquid crystal-based sensors. *Talanta*, *99*, 36-39.

[11] Yang, S., Wu, C., Tan, H., Wu, Y., Liao, S., Wu, Z., and Yu, R. (2012). Label-free liquid crystal biosensor based on specific oligonucleotide probes for heavy metal ions. *Analytical chemistry*, *85*(1), 14-18.

[12] Han, G. R., and Jang, C. H. (2014). Detection of heavy-metal ions using liquid crystal droplet patterns modulated by interaction between negatively charged carboxylate and heavy-metal cations. *Talanta*, *128*, 44-50.

[13] Bisoyi, H. K., and Kumar, S. (2011). Liquid-crystal nanoscience: an emerging avenue of soft self-assembly. *Chemical Society Reviews*, *40*(1), 306-319.

[14] Dey, A., Singh, R., and Purkait, M. K. (2014). Cobalt ferrite nanoparticles aggregated schwertmannite: A novel adsorbent for the efficient removal of arsenic. *Journal of Water Process Engineering*, *3*, 1-9.

[15] Ohe, K., Tomimatsu, R., Oshima, T., and Baba, Y. (2007). Removal of As (III) and As (V) in Groundwater Using Ferrite Adsorbents. *日本イオン交換学会誌*,*18*(4), 550-553.

[16] Khan, M., and Park, S. Y. (2014). Liquid crystal-based proton sensitive glucose biosensor. *Analytical chemistry*, *86*(3), 1493-1501.

[17] Most, D. R., VanTreeck, H. J., Grinwald, B. A., Kupcho, K. A., Sen, A., Bonds, M. D., and Acharya, B. R. (2011, February). Nematic liquid crystal interfaces for chemical and biological detection. In *SPIE OPTO* (pp. 79550L-79550L). International Society for Optics and Photonics.

[18] Choi, Y., Lee, Y., Kwon, H., and Lee, S. D. (2004). Optical detection of the ligand–receptor binding by anchoring transitions of liquid crystals. *Materials Science and Engineering: C*, *24*(1), 237-240.

[19] Zhao, Y. B., Yu, J. H., Zhao, H. F., Tong, C. Y., and Wang, P. H. (2011). A novel method for label-free detection of ricin using liquid crystals supported on chemically functionalized surfaces. *Sensors and Actuators B: Chemical*,*155*(1), 351-356.

[20] He, S., Liang, W., Tanner, C., Cheng, K. L., Fang, J., and Wu, S. T. (2013). Liquid crystal based sensors for the detection of cholic acid. *Analytical Methods*, *5*(16), 4126-4130.

[21] Srivastava, N. K., and Majumder, C. B. (2008). Novel biofiltration methods for the treatment of heavy metals from industrial wastewater. *Journal of hazardous materials*, *151*(1), 1-8.

[22] Aragay, G., Pons, J., and Merkoçi, A. (2011). Recent trends in macro-, micro-, and nanomaterial-based tools and strategies for heavy-metal detection. *Chemical reviews*, *111*(5), 3433-3458.

[23] Hojsak, I., Braegger, C., Bronsky, J., Campoy, C., Colomb, V., Decsi, T., and Molgaard, C. (2015). Arsenic in rice: a cause for concern. *Journal of pediatric gastroenterology and nutrition*, *60*(1), 142-145.

[24] Mandal, B. K., and Suzuki, K. T. (2002). Arsenic round the world: a review. *Talanta*, *58*(1), 201-235.

[25] Gundert-Remy, U., Damm, G., Foth, H., Freyberger, A., Gebel, T., Golka, K., and Hengstler, J. G. (2015). High exposure to inorganic arsenic by food: the need for risk reduction. *Archives of Toxicology*, *89*(12), 2219-2227.

[26] Karagas, M. R., Gossai, A., Pierce, B., and Ahsan, H. (2015). Drinking water arsenic contamination, skin lesions, and malignancies: a systematic review of the global evidence. *Current environmental health reports*, *2*(1), 52-68.

[27] Maharjan, M., Watanabe, C., Ahmad, S. A., and Ohtsuka, R. (2005). Arsenic contamination in drinking water and skin manifestations in lowland Nepal: the first community-based survey. *The American journal of tropical medicine and hygiene*, *73*(2), 477-479.

[28] Hegmann, T., Qi, H., and Marx, V. M. (2007). Nanoparticles in liquid crystals: synthesis, self-assembly, defect formation and potential applications. *Journal of Inorganic and Organometallic Polymers and Materials*, *17*(3), 483-508.

[29] Pena, M. E., Korfiatis, G. P., Patel, M., Lippincott, L., and Meng, X. (2005). Adsorption of As (V) and As (III) by nanocrystalline titanium dioxide. *Water Research*, *39*(11), 2327-2337.

[30] Pena, M., Meng, X., Korfiatis, G. P., and Jing, C. (2006). Adsorption mechanism of arsenic on nanocrystalline titanium dioxide. *Environmental Science & Technology*, *40*(4), 1257-1262.

[31] Tuutijärvi, T., Lu, J., Sillanpää, M., and Chen, G. (2009). As (V) adsorption on maghemite nanoparticles. *Journal of Hazardous Materials*, *166*(2), 1415-1420.

[32] Sezgin, N., Sahin, M., Yalcin, A., & Koseoglu, Y. (2013). Synthesis, Characterization and, the Heavy Metal Removal Efficiency of MFe 2 O 4 (M= Ni, Cu) Nanoparticles. *Ekoloji*, *22*(89), 89-96.

[33] Crawford, G. P. (2007). *Liquid Crystals: Frontiers in Biomedical Applications*. World Scientific.

[34] Hussain, A., Pina, A. S., and Roque, A. C. A. (2009). Bio-recognition and detection using liquid crystals. *Biosensors and Bioelectronics*, *25*(1), 1-8.

[35] Iwabata, K., Sugai, U., Seki, Y., Furue, H., and Sakaguchi, K. (2013). Applications of biomaterials to liquid crystals. *Molecules*, *18*(4), 4703-4717.

[36] Ata Alla, R. M. S. (2013). *On the Control of Nematic Liquid Crystal Alignment*.

[37] Shah, H. J. (2007). *Engineered interfaces for liquid crystal technology*.

[38] Shenoy, D. (2006). *U.S. Patent Application No. 11/307,965*.

[39] Creagh, L. T., and Kmetz, A. R. (1973). Mechanism of surface alignment in nematic liquid crystals. *Molecular Crystals and Liquid Crystals*, *24*(1-2), 59-68.

[40] Adamson, A. W. (1967). *Physical Chemistry of Surface*s (2nd edn.) Interscience. New York, 30-37.

[41] Tan, H., Li, X., Liao, S., Yu, R., and Wu, Z. (2014). Highly-sensitive liquid crystal biosensor based on DNA dendrimers-mediated optical reorientation. *Biosensors and Bioelectronics*, *62*, 84-89.

[42] Hartono, D., Lai, S. L., Yang, K. L., and Yung, L. Y. L. (2009). A liquid crystal-based sensor for real-time and label-free identification of phospholipase-like toxins and their inhibitors. *Biosensors and Bioelectronics*, *24*(7), 2289-2293.

[43] Hu, Q. Z., and Jang, C. H. (2012). Using liquid crystals for the label-free detection of catalase at aqueous–LC interfaces. *Journal of biotechnology*, *157*(1), 223-227.

[44] Carlton, R. J., Hunter, J. T., Miller, D. S., Abbasi, R., Mushenheim, P. C., Tan, L. N., and Abbott, N. L. (2013). Chemical and biological sensing using liquid crystals. *Liquid crystals reviews*, *1*(1), 29-51.

[45] Sen, A., Kupcho, K. A., Grinwald, B. A., VanTreeck, H. J., and Acharya, B. R. (2013). Liquid crystal-based sensors for selective and quantitative detection of nitrogen dioxide. *Sensors and Actuators B: Chemical*, *178*, 222-227.

[46] Cadwell, K. D., Lockwood, N. A., Nellis, B. A., Alf, M. E., Willis, C. R., and Abbott, N. L. (2007). Detection of organophosphorous nerve agents using liquid crystals supported on chemically functionalized surfaces. *Sensors and Actuators B: Chemical*, *128*(1), 91-98.

[47] Bungabong, M. L., Ong, P. B., and Yang, K. L. (2010). Using copper perchlorate doped liquid crystals for the detection of organophosphonate vapor. *Sensors and Actuators B: Chemical*, *148*(2), 420-426.

[48] Hu, Q. Z., & Jang, C. H. (2011). Liquid crystal-based sensors for the detection of heavy metals using surface-immobilized urease. *Colloids and Surfaces B: Biointerfaces*, *88*(2), 622-626.

[49] Gul, I. H., Maqsood, A., Naeem, M., and Ashiq, M. N. (2010). Optical, magnetic and electrical investigation of cobalt ferrite nanoparticles synthesized by co-precipitation route. *Journal of alloys and compounds*, *507*(1), 201-206.

[50] Hussain, Z., Zafiu, C., Küpcü, S., Pivetta, L., Hollfelder, N., Masutani, A., and Sinner, E. K. (2014). Liquid crystal based sensors monitoring lipase activity: A new rapid and sensitive method for cytotoxicity assays. *Biosensors and Bioelectronics*, *56*, 210-216.

[51] Zhang, S., Niu, H., Cai, Y., Zhao, X., and Shi, Y. (2010). Arsenite and arsenate adsorption on co-precipitated bimetal oxide magnetic nanomaterials: $MnFe_2O_4$ and $CoFe_2O_4$. *Chemical Engineering Journal*, *158*(3), 599-607.

[52] Hussain, Z., Qazi, F., Ahmed, M. I., Usman, A., Riaz, A., and Abbasi, A. D. (2016). Liquid crystals based sensing platform-technological aspects. *Biosensors and Bioelectronics*, *85*, 110-127.

[53] John, S. (2012). Liquid-crystal nanotechnology: functional targeting and superstructure development in anisotropic soft media.